
Query-Response Causal Analysis of Reaction Events in Biochemical Reaction Networks

Pavel Loskot*

ZJU-UIUC Institute, Haining, Zhejiang, China

Correspondence*:

Pavel Loskot

pavelloskot@intl.zju.edu.cn

ZJU-UIUC Institute, 718 East Haizhou Road Haining, Zhejiang 314400, China,

pavelloskot@intl.zju.edu.cn

ABSTRACT

Stochastic simulations of biochemical reaction networks generate sequences of random reaction events in order to track the evolution of chemical species counts. The trajectories of species counts are used to infer the dynamic properties of reaction networks. In this paper, well-stirred models of biochemical reaction networks are analyzed assuming instead reaction event time-series. Since the events are categorical rather than numerical variables, their analysis relies on their empirical conditional probabilities. In particular, it is proposed to identify the reaction event sub-sequences that are conditionally nearly certain or nearly uncertain as being causally related or unrelated, respectively. Moreover, since time-ordering of reactions is locally irrelevant, the event sub-sequences can be transformed into event sets or multi-sets. The appropriately defined distance metrics allows identifying equivalent event sub-sequences, which is used to implement a computationally efficient causal or anti-causal query-response mechanism for identifying the causally associated event sub-sequences. The proposed framework for analyzing the reaction event time-series is studied assuming 5 selected models of genetic networks in 5 defined numerical experiments. The models are described and simulated in BioNetGen using the open-source stochastic simulator NFsim, which had to be modified to allow recording of the history of reaction events. The generated event time-series are analyzed by Python and Matlab scripts. The whole process of data generation, analysis and visualization has been nearly fully automated using shell scripts. Such automation of data generation and processing pipelines demonstrates the opportunities for a substantial increase in the analytical productivity.

Keywords: biochemical reaction network, causal inference, dynamic system, event time-series, NFsim, query-response, state-space, stochastic simulation

1 INTRODUCTION

Biochemical reaction networks (BRNs) represent systems of chemical species that are interacting through chemical reactions. The deterministic or stochastic models of these systems must be often analyzed numerically Gillespie (2007); Wolf et al. (2010); Warne et al. (2019); Loskot et al. (2019). The objective is to generate the time trajectories of the system state represented by the copy counts or concentrations of chemical species. These trajectories reveal the dynamic properties of these systems including stability and a transition to steady-state, if it exists.

The observed copy counts can be used to solve different types of inverse problems, such as estimating the reaction rates and other parameter values Loskot et al. (2019), and inferring topology of BRNs Villaverde et al. (2013); Dang et al. (2015); Löwe et al. (2022). The inverse problems implicitly involve causal inference. In particular, a causal ordering of reactions is crucial in reconstructing the reaction pathways from time-series observations of chemical concentrations. The causal ordering can be achieved by comparing the correlation peaks, exploiting asymmetry of the conditional correlation matrix, or by evaluating the correlation network in a series of statistical independence tests Villaverde et al. (2013). Reference Dang et al. (2015) defines four main tasks for establishing the causal relationships in BRNs: visualizing consequences of perturbing a protein, finding the shortest pathway between two proteins, detecting feedback loops, and identifying common downstream path elements from several proteins.

The commonly agreed requirements for causality are that a cause must precede the effect, and the cause must contain unique information about the effect, which is not available from elsewhere Hlaváčková-Schindler et al. (2007). Alternatively, a change in cause can be detected by its effect Eichler (2011). The causality in non-linear dynamical systems can be detected from observations assuming their state-space representation Zhang et al. (2017); Runge et al. (2019). The observed copy counts in BRNs represent multivariate time-series. The causality in multivariate time-series is usually evaluated as Granger causality Hlaváčková-Schindler et al. (2007). Other notions of causality for multivariate time-series include intervention causality and structural causality Eichler (2011); Runge et al. (2019). Sims causality extends Granger causality by also accounting for non-direct causal effects. Granger causality extended to multiple features has been studied in Hmamouche et al. (2018). Granger causality is formulated in terms of conditional probability distributions in Chikahara and Fujino (2018). In particular, provided that conditioning on the observations changes the probability distribution, the corresponding random variables can be assumed to be causally related.

A comprehensive review of causal discovery in time-series data is provided in Moraffah et al. (2021) including the metrics for evaluating the causal inferences. In Soo and Rottman (2018), it is argued that causality in time-series must account for temporal trends and dependencies in order to reach the valid conclusions. Causality in multivariate time-series can be measured by spatial covariances without assuming the time domain dependencies Prill et al. (2015). The convergent cross-mapping for determining the causality in time-series data in the presence of noise and coupling is studied in Mønster et al. (2017).

Different methods for determining the direction and strength of direct linear and non-linear causal effects are compared by simulation in Papania et al. (2013). A supervised learning for determining the causal direction between random variables has been formulated in Lopez-Paz et al. (2015). A causal significance of the average contribution to an effect produced solely by a given cause has been defined in Huang and Kleinberg (2015). Such a definition of causal measure is similar to the average causal effect and the average treatment effect.

A causal framework involving structural causal modeling (SCM) has been developed in Pearl (2009). The SCM framework allows analyzing counterfactuals and potential interventions while assuming both direct and indirect effects as well as performing a ‘what-if’ analysis via so-called Do-calculus. This framework is discussed in light of the machine learning objectives in Pearl (2019). The Bayesian SCMs for time-series data are investigated in Brodersen et al. (2015). In Park and Kellis (2021), the genes causing a disease are identified by constructing a linear SCM, which is fitted to data using regression. This model is then extended with confounding effects before adding the estimated differential effects.

The causal inference involving categorical data can be performed by a series of conditional independence tests Runge et al. (2019). Information-theoretic methods are particularly useful for detecting causality between categorical variables. Extensive review of information-theoretic methods for causality in multivariate time-series can be found in Hlaváčková-Schindler et al. (2007). Methods for binary interventions with time-series observations are investigated in Samartsidis et al. (2019).

The classification of segments in time-series data can be achieved with shapelets Mueen et al. (2011). The shapelets are local, frequently reappearing patterns, which can be efficiently detected by a matrix profile algorithm Yeh et al. (2018). The matrix profile analysis relies on defining a distance metric between data sequences. Various distance metrics for evaluating similarity between data sequences are considered in Vlachos et al. (2003); Cassisi et al. (2012); Batista et al. (2013). A distance measure suitable for categorical variables such as nucleotide bases was proposed in Zielezinski et al. (2017). This metric assumes a union of short nucleotide sequences.

Mathematical models of BRNs and the corresponding methods for statistical inferences are comprehensively surveyed in Loskot et al. (2019). The algorithms for simulating models of BRNs are surveyed in Warne et al. (2019). There are many software tools available to simulate and analyze BRNs, for example, COPASI Bergmann et al. (2017), CERENA Kazerooni et al. (2016), and BioNetGen Harris et al. (2016), which is a rule-based modeling language and also an high-level interface to NFsim Sneddon et al. (2011). A tool for visualizing the causal reaction pathways is reported in Dang et al. (2015). The network-based and network-free simulations of BRNs are compared and explained in Gupta and Mendes (2018). The timescale aspects of rule-based models of BRNs are investigated in Klinke II and Finley (2012).

In this paper, the models of BRNs are newly analyzed looking at the sequences of reaction events generated by stochastic simulations. Unlike other commonly used methods, the generated sequences of molecule copy counts are discarded in our analysis of causal associations. Our main objective is to identify reaction event sub-sequences that can be considered as being causally related. This requires to detect causality between categorical random variables Loskot (2022a). It is proposed to define causality in terms of the empirical conditional probabilities of reaction event sub-sequences. In particular, it is claimed that, if one reaction sub-sequence precedes another, and the corresponding empirical conditional probability is close to 1, these reaction events are nearly certain, and they can be considered as being causally related. On the other hand, if the empirical conditional probability is close to 0, the reaction events are conditionally nearly uncertain, and they can be considered to be causally unrelated or even independent. The corresponding method of causal inference is implemented by a computationally efficient mechanism of causal or anti-causal query and response. Moreover, since exact ordering of reaction events is locally irrelevant, various distance metrics between event sub-sequences can be defined by assuming event sets and multi-sets. The event sub-sequences having zero distance can be assumed to be equivalent. The distance metrics can be used to carry out matrix profile analysis to discover common patterns in the reaction event time-series.

Numerical examples were produced in NFsim, an open-source stochastic simulator of BRNs written in C++. This software had to be modified to allow recording of the history of reaction events Loskot (2022b). The event time-series were then processed and visualized by Python and Matlab scripts. The complete pipeline of data generation, processing and visualization was automated using Bash shell-scripts. This allows generating extensive amount of numerical results with minimum required manual interventions in relatively short time. Complete numerical results for 5 selected BRN models produced in 5 experiments

are summarized in the Supplementary file; here, only selected results for Model A are presented in Section 3.

2 METHODS

The BRN is a dynamic system that can be described by a vector state, $\mathbf{y}_t \in \{0, 1, 2, \dots\}^S$, constituting the copy counts of S chemical species, which are present in the system at time t . The states undergo random transitions due to periodically reoccurring reaction events, e_t , i.e.,

$$\mathbf{y}_t = \text{BRN}(\mathbf{y}_{t-1}, e_t). \quad (1)$$

The reaction event e_t is selected at random from R chemical reactions with the probability dependent on the current state, \mathbf{y}_{t-1} . This makes the sequence of stochastic events, $\{e_t\}_t$, to be Markovian. The sequential model (1) describes the dynamics of BRN exactly, i.e., it is an exact solution of the chemical master equation Gillespie (2007). Every defined chemical reaction bind some reactants with certain products; the reactants are consumed, and the molecule counts of product increase. Since often, $R \gg S$, chemical species are involved in more than one reaction as depicted in Figure 1. The states \mathbf{y}_t are non-negative integer vectors, although its large components can be approximated as non-negative real numbers. The maximum molecule counts of all species in the system is also limited. These constraints impose dependency between successive reaction events, e_t , representing categorical or nominal random variables.

The classical analysis of BRNs assumes descriptive or inferential statistics of the state trajectory, $\{\mathbf{y}_t\}_t$. This paper departs from analyzing the molecule counts, and instead only considers the sequence of reaction events, $\{e_t\}_t$, while completely ignoring the states, \mathbf{y}_t . The first important observation is that the sequence of $(m+1)$ reaction events, $\mathbf{e}_t = (e_t, e_{t+1}, \dots, e_{t+m})$, transforming the state \mathbf{y}_t at time t into a state \mathbf{y}_{t+m} at time $(t+m)$ can be arbitrarily reordered (in time) without changing the end-state, \mathbf{y}_{t+m} . However, such reordering of reactions may temporarily violate the non-negativity constraint or other limits imposed on the states, \mathbf{y}_t . Consequently, the sub-sequences of events, \mathbf{e}_t , can be assumed to be multi-sets (the same events can appear multiple times, but the ordering is irrelevant), or they can be converted into ordinary sets (repeated events are discarded, and only unique reactions are considered). These sets or multi-sets are denoted as, \mathbf{s}_t . The event sub-sequences can be created by a sliding-window partitioning of the original event time-series as indicated in Figure 2.

The sub-sequences \mathbf{e}_t or \mathbf{s}_t of categorical random variables can be studied by assuming their probability distributions, and also by defining various distance metrics. The former approach is used to identify causal relationships, and the latter approach enables matrix profile analysis.

2.1 Causal Associations of Event Sequences

In general, given two event sub-sequences \mathbf{e}_1 and \mathbf{e}_2 of reaction events, the objective is to determine whether these sequences could be causally related. For causal learning, given a cause \mathbf{e}_1 , the task is to determine, if \mathbf{e}_2 is its effect. For anti-causal learning, given the effect \mathbf{e}_2 , the task is determine the corresponding cause \mathbf{e}_1 . The causal specificity implies that a single cause leads to a single effect, or a single effect has exactly one cause. If the cause is sufficient, then it is enough to cause or to prevent an effect, whereas a necessary cause appears in every sufficient cause Peters et al. (2017).

The first obvious condition is that, for both causal and anti-causal learning, all events in \mathbf{e}_1 representing a cause must precede all events in the possible effect \mathbf{e}_2 , i.e., the intersection, $\mathbf{e}_1 \cap \mathbf{e}_2$, must be an empty sequence. The second condition is that, if the sequences \mathbf{e}_1 and \mathbf{e}_2 are statistically independent, they cannot be causally associated. The independence can be formulated as a null-hypothesis, and then tested

using, for example, a chi-square independence test. Since the statistical tests are always evaluated with a certain level of significance, the independence test may yield false positives as well as false negatives. Moreover, in some scenarios, the independence must be tested conditioned on other random variables such as confounders.

Different strategies were considered in the literature to determine causal models of time-series data as discussed in Section 1. In general, provided that the causal effect is identifiable, it can be transformed into a probability expression containing only the observed variables Pearl (2009). However, causal effects in multiple time-series cannot be identified, provided that their SCM contains instantaneous effects Peters et al. (2017); i.e. causal networks cannot be inferred from steady-state data. The unknown causal dependencies in SCM can be replaced with conditional distributions.

Consider now an event time-series generated by the model (1). The probability of events \mathbf{e}_2 is conditionally dependent on the preceding events \mathbf{e}_1 and the sequence of states \mathbf{y}_{1-2} , which have occurred between \mathbf{e}_1 and \mathbf{e}_2 , at times t_1 and t_2 , respectively. The conditional probability of interest is,

$$\Pr(\mathbf{e}_2|\mathbf{e}_1) = \sum_{\mathbf{y}_{1-2}} \Pr(\mathbf{e}_2|\mathbf{e}_1, \mathbf{y}_{1-2}) \Pr(\mathbf{y}_{1-2}). \quad (2)$$

Removing the dependency on states \mathbf{y}_{1-2} by averaging in (2) occurs naturally, when the conditional probability between reaction events is estimated empirically as a relative frequency of occurrence of events \mathbf{e}_1 and \mathbf{e}_2 over a sufficiently long sequence of observed reaction events.

The conditional probability (2) is the likelihood that the events \mathbf{e}_1 have occurred, provided that the events \mathbf{e}_2 were observed. In order to causally relate \mathbf{e}_1 to \mathbf{e}_2 , i.e., to claim that \mathbf{e}_1 is a cause of \mathbf{e}_2 , or \mathbf{e}_2 is an effect of \mathbf{e}_1 , the Do-calculus framework of Pearl (2009) requires to enforce \mathbf{e}_1 to occur, i.e., the conditional probability, $\Pr(\mathbf{e}_2|\text{Do}(\mathbf{e}_1))$, should be assumed instead. It is the probability that specific \mathbf{e}_2 is observed, provided that \mathbf{e}_1 have been performed. In this paper, it is claimed that the limiting cases of conditional probability (2), when it is either close to 1 or close to 0, can be interpreted as interventions within the Do-calculus framework.

DEFINITION 1. *A sufficient condition for the event sub-sequences \mathbf{e}_1 and \mathbf{e}_2 , such that all events in \mathbf{e}_1 have occurred before any event in \mathbf{e}_2 , to have a cause-effect relationship is that their conditional probability, $\Pr(\mathbf{e}_2|\mathbf{e}_1) \rightarrow 1$. In such a case, \mathbf{e}_1 is said to be a cause of \mathbf{e}_2 , and equivalently, \mathbf{e}_2 is an effect of \mathbf{e}_1 . For anti-causal association, i.e., finding a cause for given effect, it is sufficient that, $\Pr(\mathbf{e}_1|\mathbf{e}_2) \rightarrow 1$.*

DEFINITION 2. *For event sub-sequences \mathbf{e}_1 and \mathbf{e}_2 not to be causally related, it is sufficient that either one or more events in \mathbf{e}_1 have occurred after any event in \mathbf{e}_2 , or their conditional probability, $\Pr(\mathbf{e}_2|\mathbf{e}_1) \rightarrow 0$, and also, $\Pr(\mathbf{e}_1|\mathbf{e}_2) \rightarrow 0$, in order to also rule out their anti-causal association.*

There are cases when \mathbf{e}_1 causes \mathbf{e}_2 , and at the same time, \mathbf{e}_2 can cause \mathbf{e}_1 . However, causal relationships are generally asymmetric, and normally, $\Pr(\mathbf{e}_2|\mathbf{e}_1) \neq \Pr(\mathbf{e}_1|\mathbf{e}_2)$. Moreover, the conditional probability $\Pr(\mathbf{e}_2|\mathbf{e}_1)$ assumed in Definition 1 as being close to 1 indicates that, given \mathbf{e}_1 , there are only a few possible event sub-sequences \mathbf{e}_2 following \mathbf{e}_1 . However and importantly, Definition 1 cannot identify all event sub-sequences \mathbf{e}_2 that are caused by \mathbf{e}_1 , nor all event sub-sequences \mathbf{e}_1 that are a cause of \mathbf{e}_2 .

In order to practically identify the pairs of event sub-sequences, which are causally related by Definition 1, the event time-series are first partitioned into sliding-window sub-sequences \mathbf{e}_t of N events, such that the time index, $t = 1, 2, \dots$, indicates the first event in the sub-sequence, \mathbf{e}_t . The sub-sequences

\mathbf{e}_t are then split into two disjoint segments \mathbf{e}_1 and \mathbf{e}_2 (omitting the time index, t , for brevity) of N_1 and $N_2 = N - N_1$ events, respectively, and they are referred to as the left and right event sub-sequences.

The number of identified causally related event sequences can be increased by assuming smaller values of N , and by introducing the notion of equivalent sub-sequences. In particular, denote as \mathbf{s}_i and \mathbf{s}_j the sets or multi-sets corresponding to the event sub-sequences \mathbf{e}_i and \mathbf{e}_j , respectively, and let d_0 be the Hamming distance between \mathbf{e}_i and \mathbf{e}_j . Assuming the equal-length sequences \mathbf{e}_i and \mathbf{e}_j , their distance can be defined in multiple ways as follows:

$$d(\mathbf{e}_i, \mathbf{e}_j) = d_0 - |\mathbf{s}_i \cup \mathbf{s}_j| \quad (3a)$$

$$d(\mathbf{e}_i, \mathbf{e}_j) = d_0 - |\mathbf{s}_i \cap \mathbf{s}_j| \quad (3b)$$

$$d(\mathbf{e}_i, \mathbf{e}_j) = d_0 - (|\mathbf{s}_i| + |\mathbf{s}_j|) \quad (3c)$$

$$d(\mathbf{e}_i, \mathbf{e}_j) = d_0 - \max(|\mathbf{s}_i|, |\mathbf{s}_j|) \quad (3d)$$

$$d(\mathbf{e}_i, \mathbf{e}_j) = \max(|\mathbf{s}_i|, |\mathbf{s}_j|) - \min(|\mathbf{s}_i|, |\mathbf{s}_j|) \quad (3e)$$

$$d(\mathbf{e}_i, \mathbf{e}_j) = \min(|\mathbf{s}_i \setminus \mathbf{s}_j|, |\mathbf{s}_j \setminus \mathbf{s}_i|). \quad (3f)$$

Hence, always, $d(\mathbf{e}_i, \mathbf{e}_j) \geq 0$ (non-negativity), $d(\mathbf{e}_i, \mathbf{e}_j) = d(\mathbf{e}_j, \mathbf{e}_i)$ (symmetry), and $|\mathbf{s}_i| \leq |\mathbf{e}_i|$, where $|\cdot|$ denotes the cardinality of a set or the sequence length.

The metrics (3a)–(3f) allow considering the distances between sub-sequences of categorical or discrete-valued variables. The distance metrics can be used to cluster sub-sequences of reaction events, which affects the frequency of occurrence estimates of the conditional probabilities considered in Definition 1, and as illustrated in Figure 3. Moreover, the distance metrics enable matrix profile analysis of the observed event time-series. The equivalence of event sub-sequences is defined as follows.

DEFINITION 3. *The event sub-sequences \mathbf{e}_i and \mathbf{e}_j are said to be equivalent, provided that their distance, $d(\mathbf{e}_i, \mathbf{e}_j) = 0$.*

2.2 Frequency Analysis of Reaction Events

The most basic analysis assumes the frequency of occurrence of individual reaction events. Denote as \hat{P}_i the estimated probability, or equivalently, the relative frequency of occurrence of reaction i in a very long sequence of observed reaction events. For simplicity, the reaction events are not separated into a steady-state and a transition to steady-state. The reaction events can be then sorted and also clustered by values \hat{P}_i . In particular, let $\hat{P}_{(1)} > \hat{P}_{(2)} > \hat{P}_{(3)} > \dots$. The disjoint clusters C_1, C_2, \dots of reaction events can be defined as,

$$C_j = \{i : \min \hat{P}_{(i)} \gg \hat{P}_{(i')}, i' \in C_{j+1} \cup C_{j+2} \cup \dots\}. \quad (4)$$

In other words, the reaction clusters are defined, so that there is a relatively large decrease in the reaction probability between subsequent clusters C_j and C_{j+1} . In all investigated BRNs, the number of such clusters was mostly equal to three, and in some cases, only two.

Furthermore, assuming again the reaction ordering, $\hat{P}_{(1)} > \hat{P}_{(2)} > \hat{P}_{(3)} > \dots$, it may be of interest to evaluate if there are a few frequently occurring reactions dominating the reaction dynamics in a BRN, or whether the reactions are more evenly distributed. Such a spread of reactions can be measured by sample

variance. It is computed for an event sub-sequence, \mathbf{e}_t , as,

$$V_R = \sum_{(i)=1}^{N_R} \left((i) - \sum_{(i)=1}^{N_R} (i) \hat{P}_{(i)} \right)^2 \hat{P}_{(i)}, \quad \sum_{(i)=1}^{N_R} \hat{P}_{(i)} = 1 \quad (5)$$

and N_R denotes the total number of reactions defined in BRN. Alternatively, consider the random variable being the fraction of reaction types that appear in the event set \mathbf{s}_t , i.e.,

$$v_t = |\mathbf{s}_t|/N_R, \quad t = 1, 2, \dots \quad (6)$$

The spread of such random variable can be measured as the median, and the quartiles Q1 and Q3.

2.3 Query-Response Causal Analysis

Discovery of causally related event sub-sequences by Definition 1 is performed in two steps. First, a distance metric is selected in order to group equivalent sub-sequences by Definition 3. Then, a histogram is obtained to estimate the conditional probabilities of event sub-sequences as their relative frequency of occurrence. Although this is a viable procedure, it is numerically very expensive, and it restricts the assumed sub-sequence length $N_1 = |\mathbf{e}_1|$ and $N_2 = |\mathbf{e}_2|$ to rather smaller values. In order to enable exploring possibly very large number of longer sliding-window sub-sequences of length $N \gg 1$, the following query-response procedures are proposed for finding causally and anti-causally related even sub-sequences, respectively. Both procedures start from creating sliding window event sub-sequences of equal length N . Each sub-sequence is then split into the first N_1 and the last $N_2 = N - N_1$ events. The procedures are depicted in Figure 4, and they consist of the following steps.

Discovery of causal event sub-sequences

1. The input query defines criteria for selecting the left sub-sequences \mathbf{e}_1 . Let Q be such a set of initial time indexes of sub-sequences \mathbf{e}_1 satisfying the query, and let \bar{Q} be the complement of Q , i.e., $Q \cup \bar{Q}$ is the set of time indexes t of all sliding-window sub-sequences \mathbf{e}_t considered.
2. The response is formed by exploring the right event sub-sequences \mathbf{e}_2 corresponding to time indexes in the set Q . The task is to find a common property or feature shared by as many selected sub-sequences \mathbf{e}_2 as possible, while such a property or feature must not be observed among any of the sub-sequences \mathbf{e}_2 with time indexes in the complement set \bar{Q} .
3. Denote such a set of time indexes of event sub-sequences, for which the property or feature identified in Step 2 is satisfied as Q^* , so that $Q^* \subseteq Q$ and $Q^* \cap \bar{Q} = \emptyset$ (empty set). The response to the query defined in Step 1 is the identified property or feature, and the set Q^* . The sub-sequences \mathbf{e}_1 and \mathbf{e}_2 associated with the set Q^* can be then assumed to be causally related.

Discovery of anti-causal event sub-sequences

1. The input query defines criteria for selecting the right sub-sequences \mathbf{e}_2 . Let Q be such a set of initial time indexes of sub-sequences \mathbf{e}_2 satisfying the query, and let \bar{Q} be the complement of Q , i.e., $Q \cup \bar{Q}$ is the set of time indexes t of all sliding-window sub-sequences \mathbf{e}_t considered.
2. The response is formed by exploring the left event sub-sequences \mathbf{e}_1 corresponding to time indexes in the set Q . The task is to find a common property or feature shared by as many selected sub-sequences \mathbf{e}_1 as possible, while such a property or feature must not be observed among any of the sub-sequences \mathbf{e}_1 with time indexes in the complement set \bar{Q} .

- Denote such a set of time indexes of event sub-sequences, for which the property or feature identified in Step 2 is satisfied as Q^* , so that $Q^* \subseteq Q$ and $Q^* \cap \bar{Q} = \emptyset$ (empty set). The response to the query defined in Step 1 is the identified property or feature, and the set Q^* . The sub-sequences e_1 and e_2 associated with the set Q^* can be then assumed to be anti-causally related.

Numerical examples considered in the next section will assume queries formulated as the minimum number of reactions from a given reaction cluster that have occurred within the left or right event sub-sequence, respectively. The corresponding responses will assume the intersection of all left or right event sub-sets s_1 or s_2 , respectively.

2.4 Matrix Profile of Event Time-Series

The canonical matrix profile effectively shows the minimum distances between constant length sub-sequences in time-series data Mueen et al. (2011). The calculation of matrix profile is greatly optimized to avoid many unnecessary computations, so it can be used for processing very long data sequences. The small values in matrix profile indicate common patterns (motifs), whereas large values point at locations of rare patterns (discords). The matrix profile can be also used to identify time instances where the distance-based sequence statistics have changed.

The choice of distance metric and the sub-sequence length are two the most important considerations in matrix profile analysis. In addition, instead of searching for the minimum distance values, the maximum distances may reveal the level of dissimilarity between different parts of time-series data. It is also useful to count multiplicities of the distance values to understand how they are distributed. However, interpreting matrix profile for categorical random variables is beyond the scope of this paper, so the numerical results are not reported here.

2.5 Numerical Implementation and Software Tools

The main goal is to simulate several models of BRNs, and record the reaction events that have occurred in the course of these simulations. There are many software tools available to simulate BRNs. For this paper, the open-source BioNetGen software was chosen to perform the stochastic simulations, mainly because many models of BRNs are available for this software. The BioNetGen program version 2.7.0 was downloaded from Blinov et al. (2021).

The BRN models for BioNetGen are described in an intuitive and efficient BNGL language Blinov et al. (2004); Harris et al. (2016). These models are stored as ordinary text files. The BNGL model description includes a list of chemical species, reaction rates and other parameters, reaction rules, quantities to be recorded as observations, and other model components. The BNGL file is processed by a Perl script distributed with BioNetGen to generate a model description file in System Biology Markup Language (SBML) format. The SBML file can be directly simulated in the open-source NFsim software written in C++ Sneddon et al. (2011); the version 1.11 was downloaded from Sneddon et al. (2012), and the modified version 1.20 was uploaded to Loskot (2022b).

There are several issues with version 1.11 of NFsim. First, it cannot record the generated reaction events, since the dynamics of BRNs so far have always been elucidated from observed copy counts rather than from reaction events. Therefore, a new software feature was added to NFsim to allow recording of generated reaction events in a separate file. Second, the original source code cannot be recompiled incrementally when only some source files have been modified, which slows down the code development significantly. Therefore, a new global make-file was created to allow incremental compilations and speed-up the code development. Third, version 1.11 of NFsim was released a decade ago in 2012, so it does

not compile under more recent versions of C++ compiler. Hence, the original source code was further refactored to remove compiling errors under a more recent version of the gcc compiler. The updated version 1.20 of NFsim is now freely available for download from Loskot (2022b).

The generated event time-series were processed and visualized by custom scripts written in Matlab and Python. The canonical matrix profile can be calculated using a Python library `stumpy` Law (2019). The overall process of performing the simulations, processing the recorded event time-series, producing the plots, and generating the \LaTeX source code for inserting figures and tables into a supplementary file was largely automated using Bash scripts.

The BNGL model files are provided in `models` folder, the Matlab and Python scripts are available in `scripts` folder, and samples of the generated event history files are stored in `data` folder of the NFsim public repository uploaded to Github Loskot (2022b).

3 RESULTS

Numerical results were produced for 5 selected models of BRNs in 4 numerical experiments. The models and experiments are detailed below. The models are labeled by letters A–E as well as their acronyms. The experiments are labeled by integers 1–4.

Each model was simulated once for 100s of simulation time, and the sequence of generated random reaction events was recorded into a comma-separated file by NFsim. The field with reaction times was removed, since it is not relevant for subsequent experiments. The event time-series were then processed and analyzed by several Matlab and Python scripts. The script names are listed in the Supplementary file including the figures and the tables generated by these scripts.

3.1 BRN Models

Model A (Multi-states): This is a rule-based model considered in Blinov et al. (2004), Colvin et al. (2009) and Colvin et al. (2010). The model represents an idealized multivalent ligand–receptor binding with multiple ligand-induced receptor aggregates. This is example of a model with lower complexity consisting of only 11 species and 20 reactions.

Model B (Chemotaxis): This model has been proposed in Hansen et al. (2008) to study chemical signaling of chemotaxis in *Escherichia coli*, and to understand signaling adaptation to changes in chemical concentrations. The receptor enzymes involved in signaling act on small assistance neighborhoods (AN) of 5 to 7 receptor homodimers. The model contains 12 species and 41 reaction rules.

Model C (Chemotaxis-ext): This model is an extended version of previous Model B. It has the updated receptor topology with 37 species, but only 32 reaction rules.

Model D (TLBR): This model is a kinetic version of the Goldstein-Perelson model of trivalent ligand-bivalent receptor (TLBR) Yang and Hlavacek (2011); Sneddon et al. (2011). The model allows predicting the distribution of ligand-receptor aggregate sizes and configurations. This is the smallest model considered consisting of only 4 species and 6 reaction rules.

Model E (Multi-sites): This is a rule-based model that was assumed in Colvin et al. (2009) and further analyzed in Colvin et al. (2010) to test and compare the rule-free simulations of BRNs. The model represents an idealized autophosphorylation of receptor tyrosine kinase (RTK) having multiple receptor binding sites. The model rules can be extracted into 68 species and 290 reactions.

Model	A	B	C	D	E
functions	-	17	11	-	-
parameters	11	55	53	22	11
groups	6	-	-	-	5
molecule types	5	-	-	4	5
species	5	12	37	4	5
ext. species	11	-	-	-	68
reaction rules	6	41	32	6	17
ext. reactions	20	-	-	-	290
ext. iterations	5	-	-	-	10

Table 1. Summary of model complexities.

Model	A	B	C	D	E
reaction events	133,513	57,621	53,457	17,238	2,353,366
reaction types	6	22	16	24	18
walk-clock time [s]	0.1	2.8	1.5	1.5	1.6

Table 2. Model simulations over 100s of simulation time.

3.2 Numerical Experiments

The numerical results presented here are selected to support the key observations. Complete numerical results that were generated for 5 BRN models in 4 experiments are provided in the Supplementary file.

Experiment 1:

The objective is to evaluate the models complexity in terms of the number of functions, species, parameters, reaction rules and molecule types (Table 1). The rule-based models A and B defined by the BNGL file can be fully extracted over several iterations in order to enumerate all combinations of reactions specified by the reaction rules. However, the reaction network extraction cannot be performed for the reaction rules defined in models B, C and D. The total number of groups, species and reactions in the extracted models A and E are also listed in Table 1.

The wall-clock times to simulate the BRN models over 100s of simulation time, the number of randomly generated reaction events, and the number of unique reactions are compared in Table 2. It demonstrates a great efficiency of network-free modeling and simulations. The reaction events are produced at the fastest rate for model E, and at the slowest rate for model D.

In addition, the recorded event history files were processed to find unique sliding-window N -tuples of reaction events and their counts (i.e., histograms). The resulting N -tuple statistics can be found in supplementary Tables S1–S5 for sliding window sub-sequences of $N = 1, 3$ and 5 reaction events, respectively. Moreover, the event time-series were split into 100 blocks of 1s duration each. For models B–E (Chemotaxis, Chemotaxis-ext, Multi-sites, and TLBR), the probabilities of reaction N -tuples are nearly constant within blocks. On the other hand, Model A (Multi-states) appears to experience a transition into a steady-state where the reaction probabilities become constant. Furthermore, the event N -tuples can be naturally clustered by assuming their frequencies of occurrence as also indicated in Tables S1–S5.

Experiment 2:

The objective is to compare the frequency of occurrence of individual reactions. The long-term probabilities of individual reactions for Model A are shown in Figure 5A, whilst for other models, they are shown in Figures S2–S5. These probabilities can be used to naturally cluster the reactions. In particular, 3

reaction clusters can be defined for Models A, B and C, but only 2 such clusters are defined for Models D and E.

Experiment 3:

This experiment evaluates how many unique reactions are occurring within the sub-sequences e_t of N reaction events. The median, the quartiles Q1 and Q3 as well as the outliers for random variables, $|e_t|/N_R$, are shown as box plots in Figure 6, for Model A, and in Figures S7–S10, for Models B–E. In general, it can be observed that the median is non-linearly and nearly monotonically increasing with the length of event N -tuples until it eventually levels-off. Interestingly, for some values N , the inter-quartile range $|Q3 - Q1|$ collapses, and the median and the quartiles Q1 and Q3 coincide.

Experiment 4:

This experiment implements query-response method to determine causal relationships between the neighboring pairs of event sub-sequences. In particular, the query here is formed by the minimum number of reactions from a selected reaction cluster that must have occurred within the left sub-sequences of N_1 reaction events. The right sub-sequences of N_2 reaction events are first converted into sets of unique reactions. These sets can be then divided into three groups. The first group contains the reaction sets from the right sub-sequences of N_2 events corresponding to the left sub-sequences of N_1 events selected by the query that do not appear in the reaction event sub-sequences outside (i.e., not selected by) the query. The second group are the reaction sets that do only appear in the right event sub-sequences outside (i.e., not selected by) the query. The third group represents the reaction sets that are shared between right sub-sequences within the query-selected as well as query-not selected right sub-sequences.

Let r_1 , r_2 and r_3 , respectively, be the relative sizes of these three groups, so that $r_1 + r_2 + r_3 = 100\%$ (see Figure 4A). The values r_1 (blue bars), r_2 (red bars) and r_3 (yellow bars) for Model A are shown as stacked bar plots in Figure 7. The experiments are labeled as “4-C-F”, where $F \geq 1$ is the required minimum number of reactions from the reaction cluster, $C \in \{1, 2, 3\}$, to have occurred in each left sub-sequence of N_1 reaction events. The complete experimental results for all models and $F = 1, 3$ and 5 are provided in Figures S11–S88 in Supplementary.

The plots in Figure 7 clearly suggest that both C and F are important parameters when formulating the query. Ideally, the size of the response (the effects) matches the size of the query (the causes). This is the case when $r_1 \rightarrow 100\%$, i.e., the responses fully cover different queries, which is indicated by full blue bars in Figure 7. When $r_2 \rightarrow 100\%$ (tall red bars in Figure 7), none or only a few responses match the queries about the effects. Such responses indicate that most of the right event sub-sequences are causally unrelated to the query. Larger r_3 values (large yellow bars) correspond to cases when none or only a few event sub-sequences in the response can be considered to be either causally related or causally unrelated to the query, so these cases have the smallest information insight.

In general, it can be concluded that larger values of N_1 , which are used to formulate the query about effects as well as larger values of N_2 , which are used to identify a common property or feature among the right event sub-sequences chosen by the query, shift the probability mass towards either causal or non-causal event sets.

Experiment 5:

This experiment expands previous Experiment 4 in order to generate causal statements that can be made about a given biochemical reaction network. Consider Model A as an example. This model represents ligand-receptor (L-R) binding in presence of adapter protein (A). The adapter protein contains tyrosine

query		query size	response size	min-max observed reactions					
n_{\min}	cluster			R1	R2	R3	R4	R5	R6
5	1	2670	919	2-24	0-20	0-11	0-8	0-3	0-3
15	1	2645	913	2-24	0-20	0-11	0-8	0-3	0-3
5	2	1267	593	3-21	0-17	0-9	0-7	0-2	0-3
10	2	46	45	5-18	1-14	0-8	0-5	0-1	0-1
1	3	824	469	3-19	2-17	0-7	0-8	0-2	0-3
3	3	17	17	6-10	10-11	1-3	2-5	0-1	0-1

Table 3. Example causal statements generated from the simulated event-series of model A for the queries of $N_1 = 25$ reaction events, and the responses of $N_2 = 25$ reaction events.

(Y), which can be in phosphorylated (P) or unphosphorylated (U) form Colvin et al. (2009). The model is referred to as being multi-site, since all species L, R and A contains dedicated binding sites (Figure 5B). There are only 6 reactions defined in this model. Specifically, R1 and R5 denote binding (forward reaction) and unbinding (reverse reaction) of ligand to receptor, respectively, whereas R2 and R6 denote binding (forward reaction) and unbinding (reverse reaction) of adapter to receptor, respectively. The phosphorylation and unphosphorylation are labeled as reactions R3 and R4, respectively. The completely expanded reaction rules are then shown in Figure 5C.

The generated causal statements are summarized in Table 3. In particular, the query representing a cause is defined as the minimum number of reactions from the given reaction cluster $C = 1, 2$ and 3 that must have occurred within the reaction sub-sub-sequences of N_1 events. The query size in Table 3 indicates how many such reaction sub-sequences satisfy this condition, while only unique sub-sequences are counted. The response representing the effect is formed by all subsequent sub-sequences of N_2 reaction events; only the unique such sub-sequences are again counted in Table 3 as the response size. In addition, the minimum and the maximum number of all 6 reactions defined in Model A contained within the response event sub-sequences are also reported in Table 3. For instance, it can be observed from Table 3 that some reactions are guaranteed to occur with certainty (non-zero minimum counts) within the query response event sub-sequences.

Experiment 6:

This experiment is similar to Experiment 4, however, now the query about causes is anti-causal as it selects the right reaction events as effects, and the returned response are the corresponding left reaction sub-sequences to be evaluated as possible reaction causes. The values l_1, l_2 and $l_3, l_1 + l_2 + l_3 = 100\%$ can be again defined to be the fractions of sizes of the left reaction event sets that are within the given query (blue bars), outside the given query (red bars), or lie in the intersection of these two groups (yellow bars), respectively, (see Figure 4B).

The experiments are labeled as “5-C-F” with the same definition for C and F . Interestingly, given C and F , the bar plots for Experiment 4 and 5 are similar but not identical. However, this is the consequence of how the queries are formulated and the responses with a common property or feature determined in our examples, rather than a general rule.

Experiment 7:

Similarly to Experiment 5, which has been used to produce causal statements for Experiment 4, Experiment 7 generates anti-causal statements for Experiment 6. Model A described in Figure 5 is again considered as an example. In particular, the query representing the effects is formed by sub-sequences of N_2 reaction events containing at least a given number of reactions from the reaction cluster $C = 1, 2$ and 3 ,

query		query size	response size	min–max observed reactions					
n_{\min}	cluster			$R1$	$R2$	$R3$	$R4$	$R5$	$R6$
5	1	2670	887	3-24	0-18	0-12	0-8	0-3	0-3
15	1	2648	884	3-24	0-18	0-12	0-8	0-3	0-3
5	2	1264	590	3-21	0-18	0-12	0-8	0-2	0-3
10	2	39	38	6-15	4-11	0-6	2-6	0-1	0-2
1	3	879	455	3-16	3-17	0-8	0-8	0-2	0-3
3	3	16	16	7-14	7-13	0-4	0-2	0-2	0-2

Table 4. Example anti-causal statements generated from the simulated event-series of model A for the queries of $N_2 = 25$ reaction events, and the responses of $N_1 = 25$ reaction events.

respectively. The preceding sub-sequences of N_1 reaction events representing the cause contain a certain minimum and maximum number of reactions as shown in Table 4. These minimum counts are sometimes non-zero, so that the corresponding reactions are guaranteed to occur within the sub-sequences of the cause.

4 DISCUSSION

In this paper, BRNs were newly analyzed using recorded traces of reaction events produced in stochastic simulations of these systems. It is a completely different strategy from the one used previously, when the dynamics of BRNs were deduced from traces of the species copy counts. Given the initial state of molecule counts, and a sequence of reaction events, the trajectory of system states can be perfectly reconstructed. This implies that the history of reaction events contains complete information for studying the system dynamics. Recording the event history also requires much less storage, since only a single reaction index needs to be recorded, whereas the complete system state can be a very large vector. However, in this paper, the main objective was to identify the causally related and causally unrelated event sub-sequences rather than to explicitly infer the system dynamics.

Knowing the reaction network does not reveal causality. Normally, the observations are changes in molecule copy counts due to randomly occurring reaction events. The method proposed in this paper allows inferring, with very high probability, the causally related as well as causally unrelated sub-sequence of reaction events by observing the event time-series. It is then possible to make causal statements such as “if the observed sub-sequence of reaction events contains a defined multiplicity of certain reactions, then, with near certainty, the subsequent sub-sequence of reactions will contain the defined number of some specified reactions”.

There are many definitions of causality in the literature. The causality in time-series and multivariate time-series were studied extensively Hlaváčková-Schindler et al. (2007); Eichler (2011); Runge et al. (2019). The basic considerations are whether statistical associations such as correlations or conditional dependencies may be sufficient to claim causality under some conditions, and whether causality can be inferred solely from observations without any prior knowledge. A short answer is that a causal discovery from data and observed statistical associations are critically dependent on the structure of data model. The event time-series described by model (1) involve categorical random variables. The Markovian property of model (1) is conditioned on the current system state, and the reaction events represent observations in such a state-space model. The events, however, can only be readily obtained in computer simulations. For in vivo and in vitro experiments, the reaction events must be inferred from the observed copy counts; in these scenarios, the role of observations and states is interchanged.

The basic methods for detecting causally related event sequences require to implement different types of interventions, or systematically perform the tests of independence. In this paper, it was proposed to identify causally related reaction event sub-sequences by either measuring their empirical conditional probabilities, or better, by defining a much more computationally efficient query-response mechanism. In particular, the sliding-window event sub-sequences were split into the left and right sub-sequences, which can be then converted into reaction event sets or multi-sets. The causal query about effects identifies a group of left reaction event sub-sequences. The corresponding right event sub-sequences are then evaluated to identify a common property or feature; it is crucial that this property or feature is not present in the right event sub-sequences that were not selected by the query. The response to the given query can be the list of event sub-sequences sharing a common property or feature. For anti-causal query about causes, the selected effects consisting of right event sub-sequences are matched with the left event sub-sequences. The search is then performed to again identify a common property or feature to be returned as causes for the given query. The reasoning in both causal and anti-causal query-response can be inverted in order to identify non-causal associations instead.

The basic idea of determining causal and non-causal relationships between reaction event sub-sequences using a query-response mechanism still relies on the conditional probability to be either very large or very small, respectively. In other words, nearly certain (uncertain) event sub-sequences can be assumed as causally related (unrelated). Furthermore, since the ordering of reaction events is locally irrelevant, the event sub-sequences can be converted into event sets or multi-sets.

One interesting and practical application of causally predicting the multiplicities of occurrences of reactions within the event sub-sequences is to facilitate an inverse problem of inferring the reaction events, which may have occurred between the measurements of chemical species concentrations. The method of causally relating the event sub-sequences can substantially constrain the number of possible reaction events that may have occurred between the two observations. This would require that the proposed method is further developed beyond the presented application of analyzing *in silico* simulations of biochemical reaction networks as considered in this paper.

The future work can consider a more systematic approach for defining more complex queries about the reaction events and effective methods for searching common properties or features among the corresponding events in the response while maintain good computational efficiency. In addition, the causal discovery may also exploit both reaction events and molecule copy counts. More importantly, once causally related or unrelated event sub-sequences have been identified, the crucial question is how to interpret such information to better understand the underlying BRNs or biological systems that they represent.

The distance metrics that were defined for event sequences, sets or multi-sets allow to define equivalences between events, and to perform the matrix profile analysis. The matrix profile can be conceptually modified to not only show the minimum distance values, but also to compute the maxima and any other statistics of the distance metrics including multiplicities of these values. This resembles a feature extraction process when the original time-series data are transformed into another time-series representation. Unfortunately, at present, the libraries implementing the canonical matrix profile are optimized only for the Euclidean distance.

The NFsim software can be further modified. For instance, it is desirable to remove unused or rarely used features from the source code, and refactor the source code for better readability, speed and efficiency. In addition, it would be extremely useful to provide a highly optimized implementation of the matrix profile

algorithm allowing for arbitrary distance metrics and other statistics. There is also a need to have a general computing framework for fast, sliding-window processing of multivariate time-series data in Python and in other languages. Lastly, as demonstrated in this paper, the data processing and visualization can be readily automated, however, automating also interpretation of the produced results is a much harder but also much more interesting problem to consider.

5 CONCLUSION

The event time-series generated by stochastic simulations of BRNs were used to discover causally related event sub-sequences. The causality was defined in terms of conditionally certain and uncertain reaction events. Causal, non-causal and anti-causal associations were determined by a computationally efficient query-response mechanism. In addition, since the ordering of reaction events is locally irrelevant, the event sub-sequences can be transformed into event sets or multi-sets. This can be exploited in defining various distance metrics between event sequences. The event sequences having zero distance can be assumed to be equivalent. The sequence equivalence increases the likelihood of identifying the causally related events. The defined distance metrics can be also used in the extended matrix profile analysis of event time-series.

Producing numerical results required to modify and update the popular stochastic simulator of BRNs NFsim. The reaction event time-series from simulations of 5 models of BRNs were processed by Python and Matlab scripts in 5 numerical experiments. All tables and figures automatically generated by the scripts are summarized in Supplementary, whereas only selected results are presented in the main paper.

ACKNOWLEDGMENT

This work was supported by a research grant from Zhejiang University.

CONFLICT OF INTEREST STATEMENT

The author declares that the research was conducted in the absence of any commercial or financial relationships that could be construed as a potential conflict of interest.

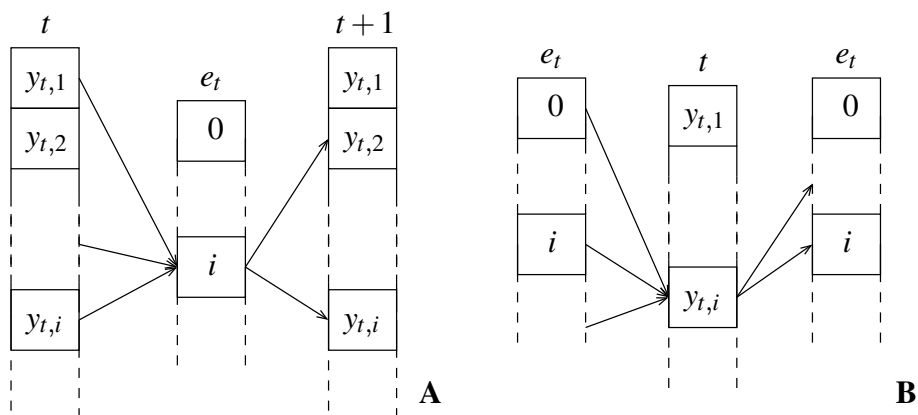


Figure 1. The causal associations between chemical species and chemical reactions in a BRN; a reaction event-centric model (A), and a chemical species count-centric model (B).

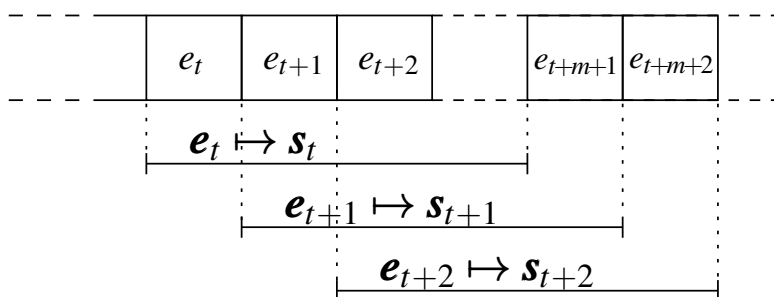


Figure 2. The sliding-window event sub-sequences, e_t , of $(m + 1)$ events mapped into event multi-sets or ordinary sets, s_t .

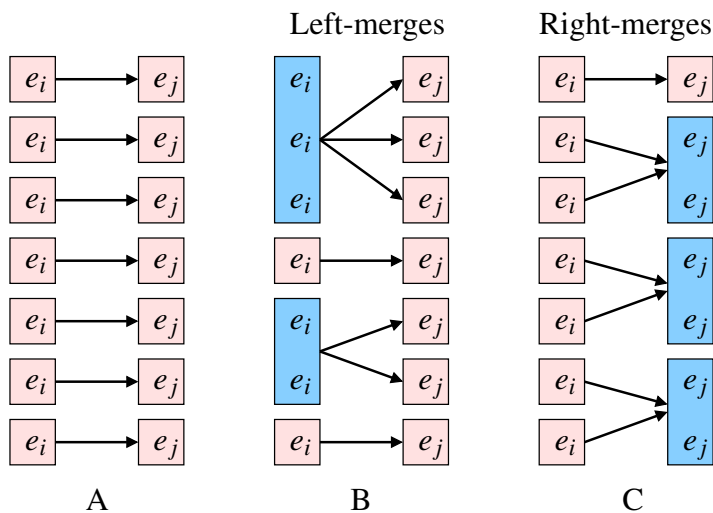


Figure 3. The original pairs of unique event sub-sequences (A), merging equivalent left event sub-sequences as potential causes (B), and merging equivalent right event sub-sequences as potential effects (C). The event sub-sequences are equivalent, if their suitably defined distance is zero.

FIGURES

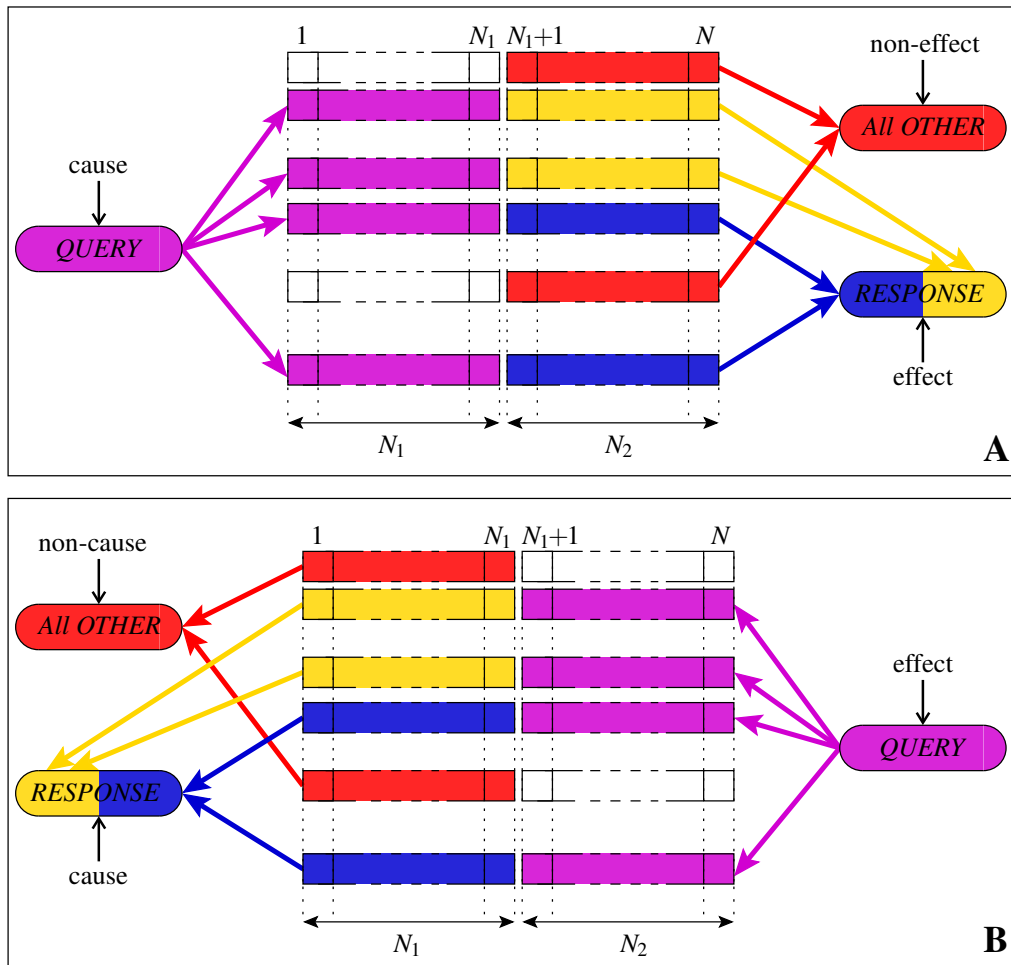


Figure 4. The causal (anti-causal) inference over reaction event sub-sequences is performed by formulating a query to select the event sub-sequences representing a cause (effect). The response to the query is a collection of event sub-sequences representing the effect (cause), for which some shared feature can be identified. This feature is then used to formulate a causal or anti-causal statement about a biochemical reaction network. A query-response causal (A) and anti-causal (B) discovery of cause-effect relationships between the left and right event sub-sequences of N_1 and $N_2 = (N - N_1)$ reaction events, respectively. The responses corresponding to the queried sub-sequences (magenta boxes) are divided into sub-sequences that can be described by some defined shared property or feature (blue boxes) and those that cannot (yellow boxes). Ideally, the number of yellow boxes is very small, or even zero.

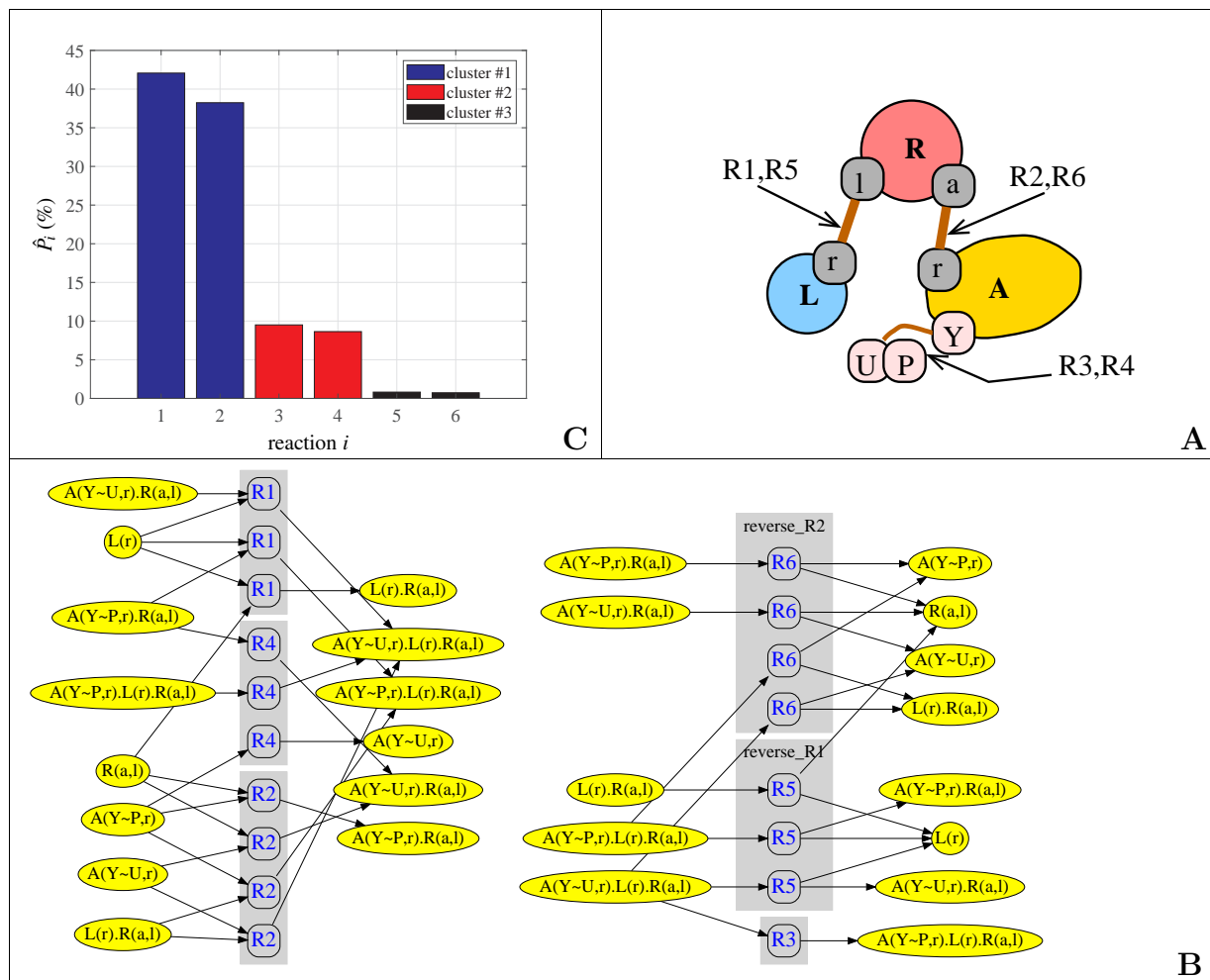


Figure 5. Model A is an example of a reaction network with multi-site chemical species (panel A). It models ligand-receptor (L-R) binding in the presence of adapter protein (A). The adapter protein contains tyrosine (Y), which can be in phosphorylated (P) or unphosphorylated (U) state. The expanded reaction rules R1–R6 are shown in (panel B). The long-term probability of individual reactions (panel C). The reactions can be naturally clustered into 3 groups.

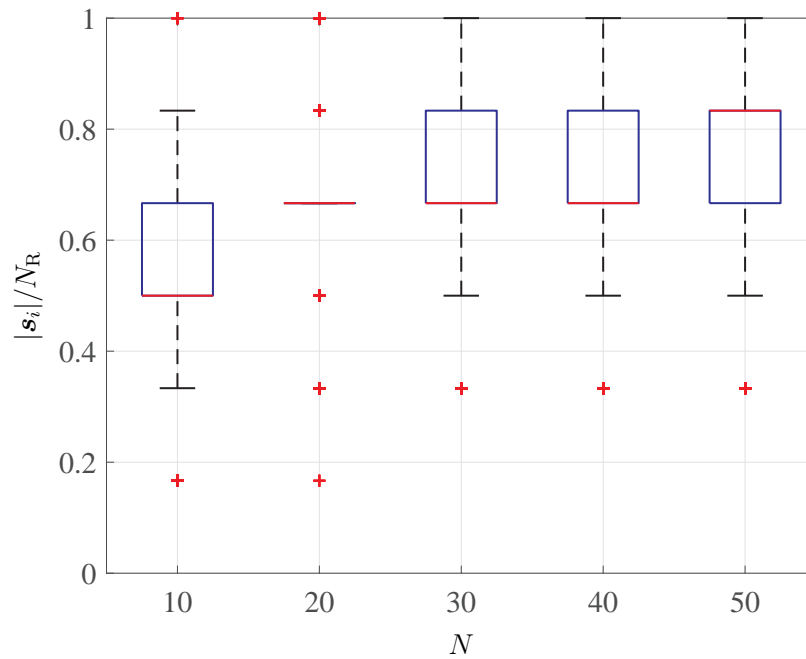


Figure 6. The box plot of relative frequency occurrences of unique reactions in Model A showing the median, quartiles $Q1$ and $Q3$, and the outliers outside the $1.5 \times |Q3 - Q1|$ range. The reaction event sub-sequences, e_i , were converted first into multi-sets, s_i .

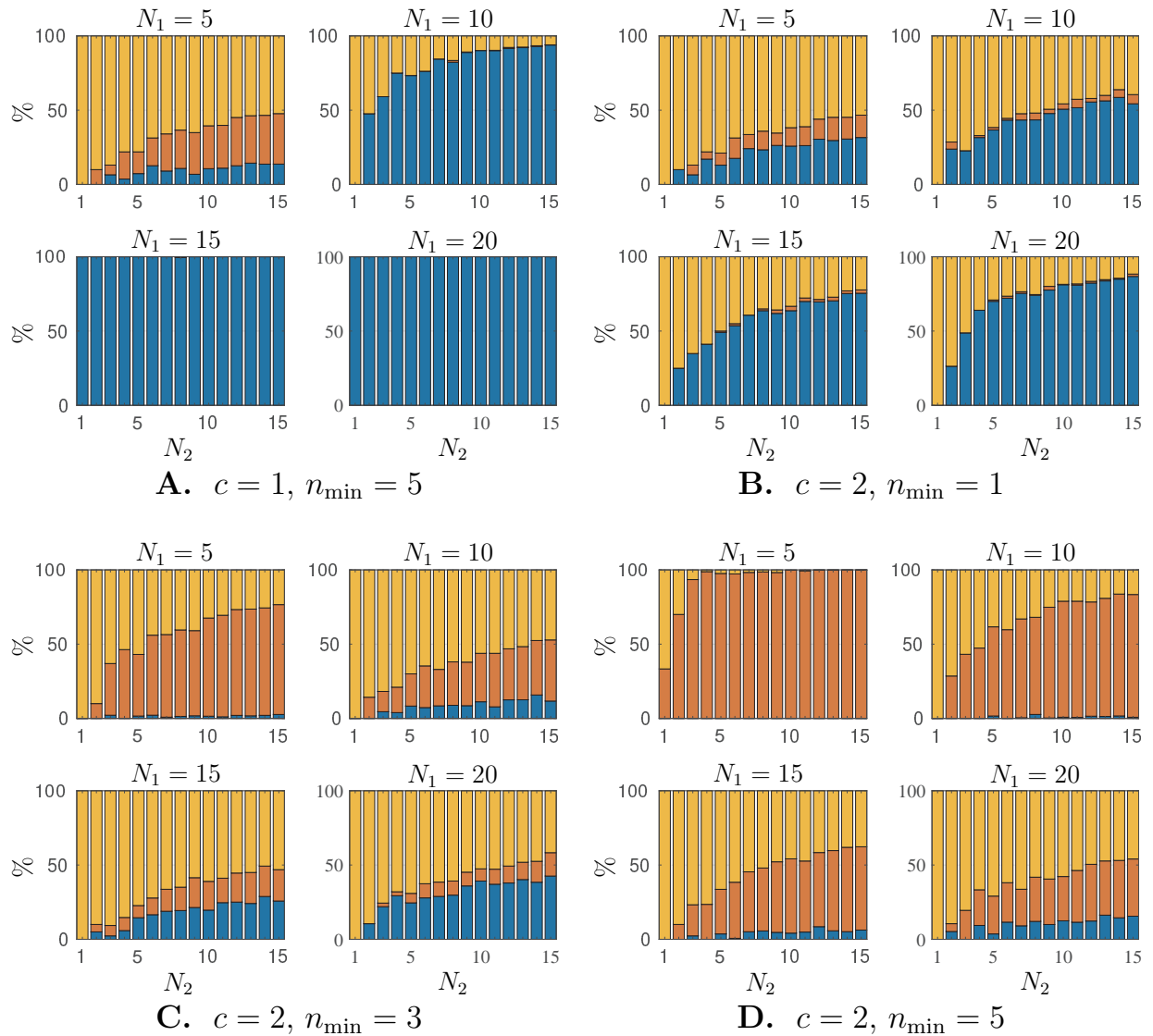


Figure 7. The bar plots for Model A quantifying the responses to a given causal query defined as all sub-sequences of $N_1 = 5, 10, 15$ and 20 reaction events, respectively, containing at least n_{\min} reaction events from the reaction group, $c \in \{1, 2, 3\}$. The length N_2 of the response sub-sequences (the effects) is varied between 1 and 15 . The blue bars are fractions of the response sub-sequences to the given causal query. The red bars are fractions of sub-sequences outside the causal query. The yellow bars are the response sub-sequences, which are shared between the response sub-sequences contained within and outside the given causal query, respectively. This coloring scheme corresponds to the one used in Figure 4.

REFERENCES

- Batista, G. E., Keogh, E. J., Tataw, O. M., and Souza, V. M. (2013). CID: an efficient complexity-invariant distance for time series. *Data Mining and Knowledge Discovery* 28, 634–669. doi: 10.1007/s10618-013-0312-3
- Bergmann, F. T., Hoops, S., Klahn, B., Kummer, U., Mendes, P., Pahle, J., et al. (2017). COPASI and its applications in biotechnology. *Journal of Biotechnology* 261, 215–220. doi: 10.1016/j.jbiotec.2017.06.1200
- Blinov, M. L., Faeder, J. R., Goldstein, B., and Hlavacek, W. S. (2004). Software for rule-based modeling of signal transduction based on the interactions of molecular domains. *Bioinformatics* 20, 3289–3291. doi: 10.1093/bioinformatics/bth378
- Blinov, M. L., Faeder, J. R., Hlavacek, W. S., Goldstein, B., Hogg, J., Harris, L., et al. (2021). BioNetGen source code, version 2.7.0. <https://github.com/RuleWorld/bionetgen>
- Brodersen, K. H., Gallusser, F., Koehler, J., Remy, N., and Scott, S. L. (2015). Inferring causal impact using Bayesian structural time-series models. *The Annals of Applied Statistics* 9, 247–274. doi: 10.1214/14-AOAS788
- Cassisi, C., Montalto, P., Aliotta, M., Cannata, A., and Pulvirenti, A. (2012). *Similarity Measures and Dimensionality Reduction Techniques for Time Series Data Mining* (IntechOpen, London, UK). 71–96. doi: 10.5772/49941
- Chikahara, Y. and Fujino, A. (2018). Causal inference in time series via supervised learning. In *IJCAI'18*. 2042–2048. doi: 10.5555/3304889.3304943
- Colvin, J., Monine, M. I., Faeder, J. R., Hlavacek, W. S., Hoff, D. D. V., and Posner, R. G. (2009). Simulation of large-scale rule-based models. *Bioinformatics* 25, 910–917. doi: 10.1093/bioinformatics/btp066
- Colvin, J., Monine, M. I., Gutenkunst, R. N., Hlavacek, W. S., Hoff, D. D. V., and Posner, R. G. (2010). RuleMonkey: software for stochastic simulation of rule-based models. *BMC Bioinformatics* 11, 1–14. doi: 10.1186/1471-2105-11-404
- Dang, T. N., Murray, P., Aurisano, J., and Forbes, A. G. (2015). ReactionFlow: an interactive visualization tool for causality analysis in biological pathways. *BMC Proceedings* 9, 1–18. doi: 10.1186/1753-6561-9-S6-S6
- Eichler, M. (2011). *Causal Inference in Time Series Analysis* (Wiley), chap. In Causality (eds W.A. Shewhart et al.). doi: 10.1002/9781119945710.ch22
- Gillespie, D. T. (2007). Stochastic simulation of chemical kinetics. *Annual Review of Physical Chemistry* 58, 35–55. doi: 10.1146/annurev.physchem.58.032806.104637
- Gupta, A. and Mendes, P. (2018). An overview of network-based and -free approaches for stochastic simulation of biochemical systems. *Computation* 6, 1–20. doi: 10.3390/computation6010009
- Hansen, C. H., Endres, R. G., and Wingreen, N. S. (2008). Chemotaxis in *Escherichia coli*: A molecular model for robust precise adaptation. *PLOS Computational Biology* 4, 0014–0027. doi: 10.1371/journal.pcbi.0040001
- Harris, L. A., Hogg, J. S., Tapia, J.-J., Sekar, J. A. P., Gupta, S., Korsunsky, I., et al. (2016). Bionetgen 2.2: advances in rule-based modeling. *Bioinformatics* 32, 3366–3368. doi: 10.1093/bioinformatics/btw469
- Hlaváčková-Schindlerová, K., Paluš, M., Vejmelka, M., and Bhattacharya, J. (2007). Causality detection based on information-theoretic approaches in time series analysis. *Physics Reports* 441, 1–46. doi: 10.1016/j.physrep.2006.12.004
- Hmamouche, Y., Casali, A., and Lakhali, L. (2018). A causality based feature selection approach for multivariate time series forecasting. In *DBKDA*. 1–6

- Huang, Y. and Kleinberg, S. (2015). Fast and accurate causal inference from time series data. In *Int. Florida AI Research Soc. Conf.* 1–6
- Kazeroonian, A., Fröhlich, F., Raue, A., Theis, F. J., and Hasenauer, J. (2016). CERENA: ChEmical REaction Network Analyzer — A toolbox for the simulation and analysis of stochastic chemical kinetics. *PLoS ONE* 11, 1–15. doi: 10.1371/journal.pone.0146732
- Klinke II, D. J. and Finley, S. D. (2012). Timescale analysis of rule-based biochemical reaction networks. *Biotechnology Prog.* 28, 33–44. doi: 10.1002/btpr.704
- Law, S. M. (2019). STUMPY: A powerful and scalable Python library for time series data mining. *Journal of Open Source Software* 4, 1504
- Lopez-Paz, D., Muandet, K., Schölkopf, B., and Tolstikhin, I. (2015). Towards a learning theory of cause-effect inference. In *ICML'15*. vol. 37, 1452–1461. doi: 10.5555/3045118.3045273
- Loskot, P. (2022a). Discovering causality in event time-series. In *SIGNAL 2022*. 18–23
- Loskot, P. (2022b). NFsim source code, version 1.20. <https://github.com/ploskot/nfsim>
- Loskot, P., Atitey, K., and Mihaylova, L. (2019). Comprehensive review of models and methods for inferences in bio-chemical reaction networks. *Frontiers in Genetics* 10, 1–29. doi: 10.3389/fgene.2019.00549
- Löwe, S., Madras, D., Zemel, R., and Welling, M. (2022). Amortized causal discovery: Learning to infer causal graphs from time-series data. ArXiv:2006.10833 [cs.LG]
- Mønster, D., Fusaroli, R., Tylén, K., Roepstorff, A., and Sherson, J. F. (2017). Causal inference from noisy time-series data – testing the convergent cross-mapping algorithm in the presence of noise and external influence. *Future Generation Computer Systems* 73, 52–62. doi: 10.1016/j.future.2016.12.009
- Moraffah, R., Sheth, P., Karami, M., Bhattacharya, A., Wang, Q., Tahir, A., et al. (2021). Causal inference for time series analysis: problems, methods and evaluation. *Knowledge and Information Systems* 63, 3041–3085. doi: 10.1007/s10115-021-01621-0
- Mueen, A., Keogh, E., and Young, N. (2011). Logical-shapelets: An expressive primitive for time series classification. In *ACM SIGKDD*. 1154–1162. doi: 10.1145/2020408.2020587
- Papana, A., Kyrtsov, C., Kugiumtzis, D., and Diks, C. (2013). Simulation study of direct causality measures in multivariate time series. *Entropy* 15, 2635–2661. doi: 10.3390/e15072635
- Park, Y. P. and Kellis, M. (2021). CoCoA-diff: counterfactual inference for single-cell gene expression. *Genome Biology* 22, 1–23. doi: 10.1186/s13059-021-02438-4
- Pearl, J. (2009). Causal inference in statistics: An overview. *Statistics Surveys* 3, 96–146. doi: 10.1214/09-SS057
- Pearl, J. (2019). The seven tools of causal inference, with reflections on machine learning. *Communications of the ACM* 62, 54–60. doi: 10.1145/3241036
- Peters, J., Janzing, D., and Schölkopf, B. (2017). *Elements of Causal Inference* (The MIT Press, Cambridge, Massachusetts)
- Prill, R. J., Vogel, R., Cecchi, G. A., Altan-Bonnet, G., and Stolovitzky, G. (2015). Noise-driven causal inference in biomolecular networks. *PLoS ONE* 10, 1–16. doi: 10.1371/journal.pone.0125777
- Runge, J., Bathiany, S., Bollt, E., Camps-Valls, G., Coumou, D., Deyle, E., et al. (2019). Inferring causation from time series in Earth system sciences. *Nature Communications* 10, 1–13. doi: 10.1038/s41467-019-10105-3
- Samartsidis, P., Seaman, S. R., Presanis, A. M., Hickman, M., and Angelis, D. D. (2019). Assessing the causal effect of binary interventions from observational panel data with few treated units. *Statistical Science* 34, 486–503. doi: 10.1214/19-STS713

- Sneddon, M. W., Faeder, J. R., and Emonet, T. (2011). Efficient modeling, simulation and coarse-graining of biological complexity with NFsim. *Nature Methods* 8, 177–183. doi: 10.1038/nmeth.1546
- Sneddon, M. W., Hogg, J. S., Faeder, J. R., and Emonet, T. (2012). NFsim source code, version 1.11. <https://github.com/msneddon/nfsim>
- Soo, K. W. and Rottman, B. M. (2018). Causal strength induction from time series data. *Journal of Experimental Psychology: General* 147, 485–513. doi: 10.1037/xge0000423
- Villaverde, A. F., Ross, J., and Banga, J. R. (2013). Reverse engineering cellular networks with information theoretic methods. *Cells* 2, 306–329. doi: 10.3390/cells2020306
- Vlachos, M., Hadjieleftheriou, M., Gunopulos, D., and Keogh, E. (2003). Indexing multi-dimensional time-series with support for multiple distance measures. In *KDD'03*. 216–225. doi: 10.1145/956750.956777
- Warne, D. J., Baker, R. E., and Simpson, M. J. (2019). Simulation and inference algorithms for stochastic biochemical reaction networks: from basic concepts to state-of-the-art. *J. Royal Society Interface* 16, 1–20. doi: 10.1098/rsif.2018.0943
- Wolf, V., Goel, R., Mateescu, M., and Henzinger, T. A. (2010). Solving research article the chemical master equation using sliding windows. *BMC Systems Biology* 4, 1–19. doi: 10.1186/1752-0509-4-42
- Yang, J. and Hlavacek, W. S. (2011). Efficiency of reactant site sampling in network-free simulation of rule-based models for biochemical systems. *Physical Biology* 8, 055009. doi: 10.1088/1478-3975/8/5/055009
- Yeh, C.-C. M., Zhu, Y., Ulanova, L., Begum, N., Ding, Y., Dau, H. A., et al. (2018). Time series joins, motifs, discords and shapelets: a unifying view that exploits the matrix profile. *Data Mining and Knowledge Discovery* 32, 83–123. doi: 10.1007/s10618-017-0519-9
- Zhang, B.-G., Li, W., Shi, Y., Liu, X., and Chen, L. (2017). Detecting causality from short time-series data based on prediction of topologically equivalent attractors. *BMC Systems Biology* 11, 141–150. doi: 10.1186/s12918-017-0512-3
- Zielezinski, A., Vinga, S., Almeida, J., and Karlowski, W. M. (2017). Alignment-free sequence comparison: benefits, applications, and tools. *Genome Biology* 18, 1–17. doi: 10.1186/s13059-017-1319-7

Supplementary Material

The numerical results were generated for 5 biochemical models labeled as A–E in 7 experiments labeled as 1–7.

The files are available at GitHub repository <https://github.com/ploskot/nfsim/tree/update>:

- data/ sample history files produced from a single run of stochastic simulation
- models/ model definitions as BNGL files
- scripts/ Python and Matlab scripts for experiments

BIOCHEMICAL MODELS

Model A: a multi-states system defined in `models/modelA.bngl`

Blinov, M. L., Faeder, J. R., Goldstein, B., and Hlavacek, W. S. (2004). Software for rule-based modeling of signal transduction based on the interactions of molecular domains. *Bioinformatics* 20, 3289–3291. doi: 10.1093/bioinformatics/bth378

Colvin, J., Monine, M. I., Faeder, J. R., Hlavacek, W. S., Hoff, D. D. V., and Posner, R. G. (2009). Simulation of large-scale rule-based models. *Bioinformatics* 25, 910–917. doi: 10.1093/bioinformatics/btp066

Model B: a model of chemotaxis defined in `models/modelB.bngl`

Hansen, C. H., Endres, R. G., and Wingreen, N. S. (2008). Chemotaxis in *Escherichia coli*: A molecular model for robust precise adaptation. *PLOS Computational Biology* 4, 0014–0027. doi: 10.1371/journal.pcbi.0040001

Model C: an extended model of chemotaxis defined in `models/modelC.bngl`

Hansen, C. H., Endres, R. G., and Wingreen, N. S. (2008). Chemotaxis in *Escherichia coli*: A molecular model for robust precise adaptation. *PLOS Computational Biology* 4, 0014–0027. doi: 10.1371/journal.pcbi.0040001

Model D: a model of trivalent ligand-bivalent receptor defined in `models/modelD.bngl`

Sneddon, M. W., Faeder, J. R., and Emonet, T. (2011). Efficient modeling, simulation and coarse-graining of biological complexity with Nfsim. *Nature Methods* 8, 177–183. doi: 10.1038/nmeth.1546

Yang, J. and Hlavacek, W. S. (2011). Efficiency of reactant site sampling in network-free simulation of rule-based models for biochemical systems. *Physical Biology* 8, 055009. doi: 10.1088/1478-3975/8/5/055009

Model E: a multi-sites system defined in `models/modelE.bngl`

Colvin, J., Monine, M. I., Faeder, J. R., Hlavacek, W. S., Hoff, D. D. V., and Posner, R. G. (2009). Simulation of large-scale rule-based models. *Bioinformatics* 25, 910–917. doi: 10.1093/bioinformatics/btp066

Colvin, J., Monine, M. I., Gutenkunst, R. N., Hlavacek, W. S., Hoff, D. D. V., and Posner, R. G. (2010). RuleMonkey: software for stochastic simulation of rule-based models. *BMC Bioinformatics* 11, 1–14. doi: 10.1186/1471-2105-11-404

EXPERIMENTS

Experiment 1: Python scripts `script1.py` and `script2.py`

Objective: find unique reaction N -tuples and their counts, so they can be clustered by their frequency of occurrence; in addition, the N -tuple statistics assume partitioning of events into 100 blocks of 1 second duration, and the minimum and maximum values across blocks are reported

Output: Tables S5–S9

Experiment 2: Matlab script `mscript1.m`

Objective: sort and cluster reactions by their frequency of occurrence

Output: Figures 8–12

Experiment 3: Matlab script `mscript2.m`

Objective: the box plots of unique reactions within sliding-window event N -tuples to visualize their statistics; it is assumed that reactions are sorted by their frequency of occurrence as in Figures 8–12

Output: Figures 13–17

Experiment 4: Matlab script `mscript3.m`

Objective: assessment of reaction N_2 -tuples as effects for the query about N_1 -tuple as causes; the experiments and figures are labeled by the query, i.e., “ $4 - C - F$ ”, where $F \geq 1$ is the required minimum number of reactions from the reaction cluster $C \in \{1, 2, \dots\}$ occurring within reaction N_1 -tuples

Output: Figures 18–95

Experiment 5: Matlab script `mscript4.m`

Objective: generate causal statements for Experiment 4

Output: Table 3 in the main text

Experiment 6: Matlab script `mscript5.m`

Objective: assessment of reaction N_1 -tuples as causes for the query about N_2 -tuples as effects; the experiments and figures are labeled by the query, i.e., “ $5 - C - F$ ”, where $F \geq 1$ is the required minimum number of reactions from the reaction cluster $C \in \{1, 2, \dots\}$ occurring within reaction N_2 -tuples

Output: Figures 18–95

Experiment 7: Matlab script `mscript6.m`

Objective: generate anti-causal statements for Experiment 6

Output: Table 4 in the main text

N -tuple	Cluster	Uniq. tuples	Min freq.	Max freq.	Tuples total
$N = 1$	1	1–2	457–5618	473–5618	930–5618
	2	1–2	85–1281	92–1281	177–1281
	3	1–2	5–473	7–473	8–473
	4	1–1	1–126	1–126	1–126
	5	1–1	13–13	13–13	13–13
	6	1–1	1–1	1–1	1–1
$N = 3$	1	1–8	55–3355	74–3355	559–3355
	2	3–62	3–759	20–764	370–2284
	3	4–32	2–154	2–188	8–1026
	4	5–39	1–57	1–64	14–303
	5	16–44	1–3	1–38	20–505
	6	8–27	1–2	1–2	16–27
	7	21–21	1–1	1–1	21–21
$N = 5$	1	1–153	3–2090	15–2090	32–2090
	2	5–109	2–457	2–486	114–2349
	3	10–346	1–104	1–130	142–1153
	4	5–304	1–58	1–72	188–331
	5	138–266	1–3	1–40	266–1194
	6	78–78	2–2	2–2	156–156
	7	235–235	1–1	1–1	235–235

Table S5. Model A, clusters of reaction N -tuples

<i>N</i> -tuple	Cluster	Uniq. tuples	Min freq.	Max freq.	Tuples total
<i>N</i> = 1	1	1–22	6–537	42–539	62–1076
	2	1–19	3–64	14–123	25–1278
	3	1–15	1–40	1–42	1–294
	4	1–14	1–13	1–24	1–174
	5	1–7	1–5	1–9	1–53
	6	1–2	1–2	1–2	1–2
<i>N</i> = 3	1	1–283	3–21	8–27	12–1604
	2	1–186	2–12	2–14	12–372
	3	46–540	1–3	1–8	92–540
	4	59–259	1–2	1–2	118–259
	5	218–218	1–1	1–1	218–218
<i>N</i> = 5	1	1–29	2–5	2–5	3–83
	2	4–577	1–3	1–3	12–577
	3	15–2169	1–2	1–2	30–2169
	4	517–541	1–1	1–1	517–541

Table S6. Model B, clusters of reaction *N*-tuples

<i>N</i> -tuple	Cluster	Uniq. tuples	Min freq.	Max freq.	Tuples total
<i>N</i> = 1	1	2–16	7–538	40–548	155–1086
	2	1–13	5–148	5–180	5–960
	3	1–2	7–85	7–98	7–183
	4	1–5	3–38	3–51	3–218
	5	1–1	17–17	17–17	17–17
<i>N</i> = 3	1	1–267	3–17	8–43	12–1895
	2	38–127	2–3	2–11	76–276
	3	37–313	1–2	1–2	74–313
	4	132–192	1–1	1–1	132–192
<i>N</i> = 5	1	1–43	2–6	2–6	3–141
	2	2–552	1–3	1–3	6–552
	3	18–1931	1–2	1–2	36–1931
	4	377–487	1–1	1–1	377–487

Table S7. Model C, clusters of reaction *N*-tuples

<i>N</i> -tuple	Cluster	Uniq. tuples	Min freq.	Max freq.	Tuples total
<i>N</i> = 1	1	1-24	3-21	10-31	14-330
	2	1-22	1-9	1-11	1-146
	3	1-6	1-6	1-6	1-13
	4	1-4	1-3	1-3	1-6
	5	1-4	1-1	1-1	1-4
<i>N</i> = 3	1	1-206	1-3	1-3	2-206
	2	6-319	1-2	1-2	12-319
	3	146-321	1-1	1-1	146-321
<i>N</i> = 5	1	1-334	1-2	1-2	2-334
	2	332-332	1-1	1-1	332-332

Table S8. Model D, clusters of reaction *N*-tuples

<i>N</i> -tuple	Cluster	Uniq. tuples	Min freq.	Max freq.	Tuples total
<i>N</i> = 1	1	6-12	1775-6391	1889-7173	22221-40805
	2	1-6	21-1674	36-2144	47-11491
	3	1-5	21-116	21-137	21-373
	4	3-3	29-29	33-33	94-94
<i>N</i> = 3	1	27-1741	3-222	24-280	6725-23459
	2	5-1767	2-3	2-148	15-44984
	3	46-596	1-2	1-2	92-596
	4	472-588	1-1	1-1	472-588
<i>N</i> = 5	1	12-2695	3-3	3-33	36-13087
	2	816-5051	2-2	2-2	1632-10102
	3	20738-29570	1-1	1-1	20738-29570

Table S9. Model E, clusters of reaction *N*-tuples

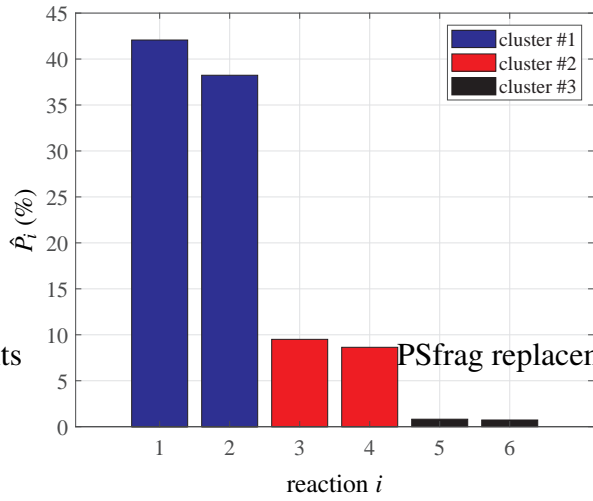


Figure 8. Model A, reaction frequency

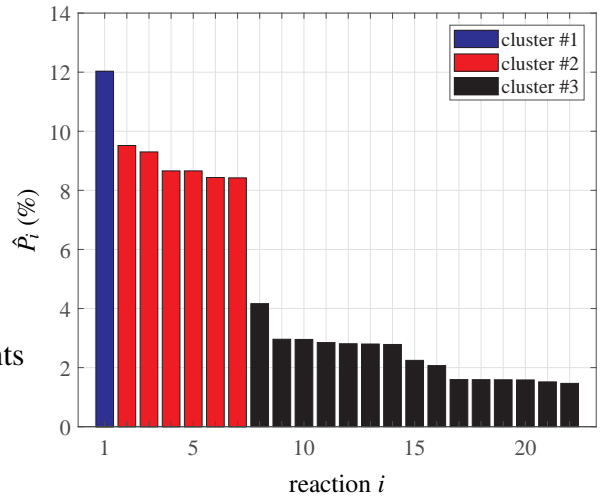


Figure 9. Model B, reaction frequency

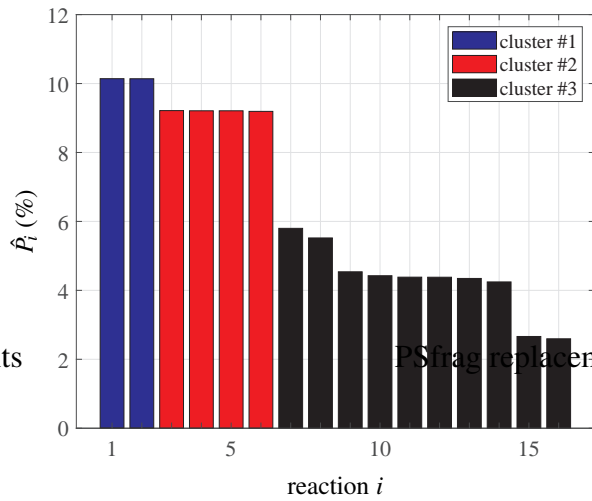


Figure 10. Model C, reaction frequency

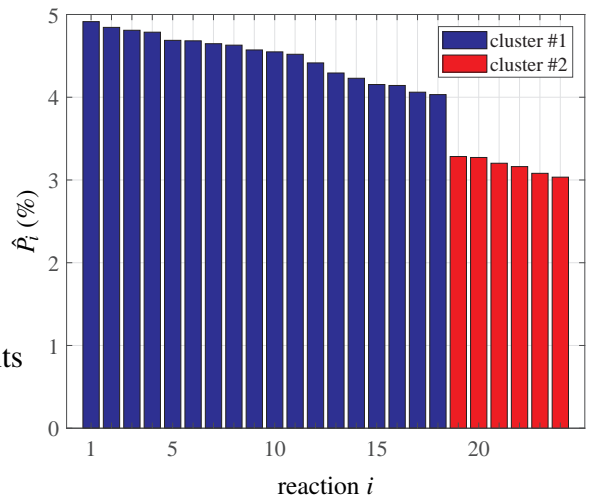


Figure 11. Model D, reaction frequency

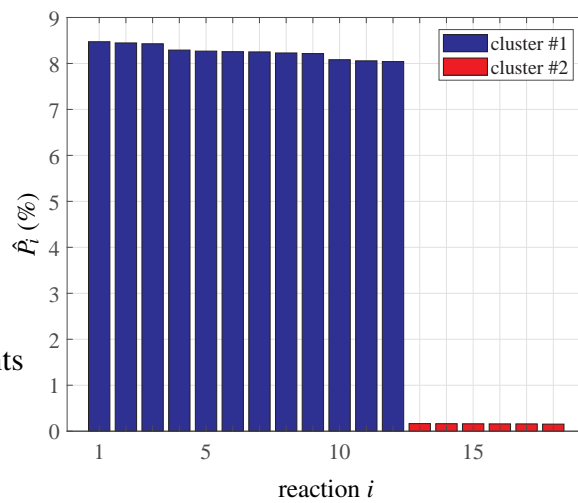


Figure 12. Model E, reaction frequency

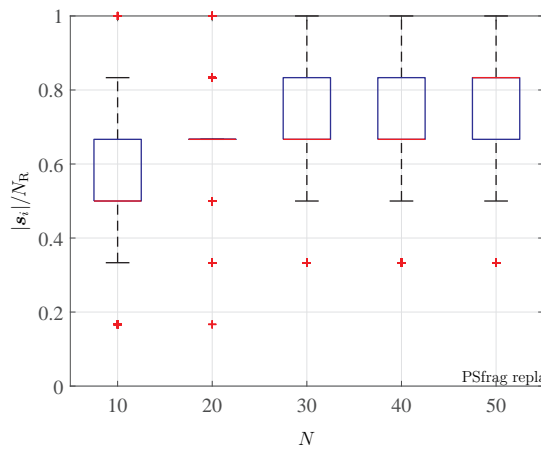


Figure 13. Model A, reaction statistics

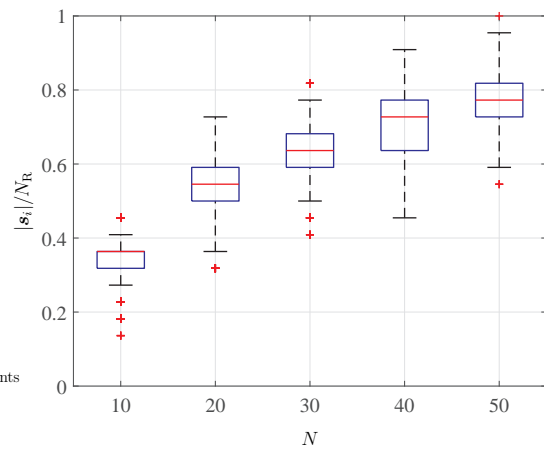


Figure 14. Model B, reaction statistics

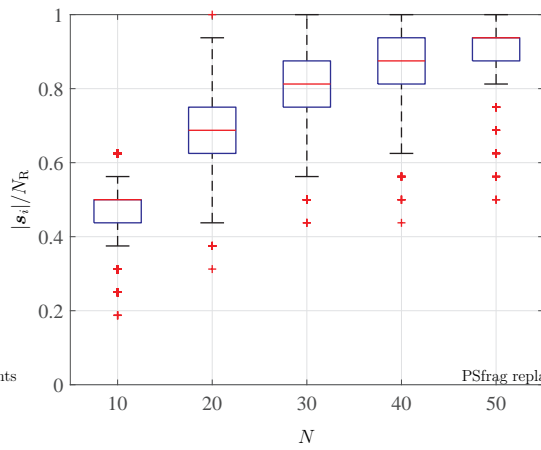


Figure 15. Model C, reaction statistics

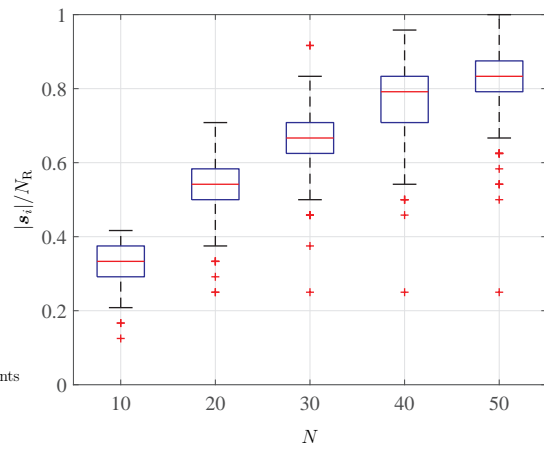


Figure 16. Model D, reaction statistics

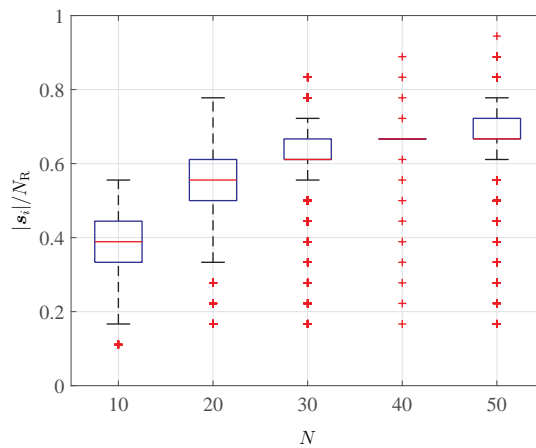


Figure 17. Model E, reaction statistics

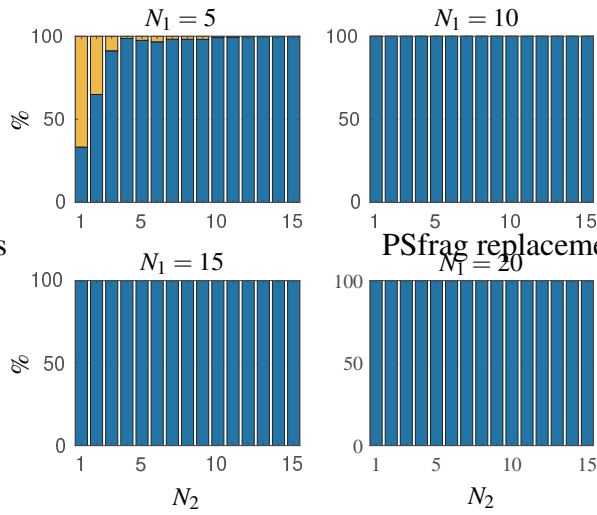


Figure 18. Model A, Experiment 4-1-1

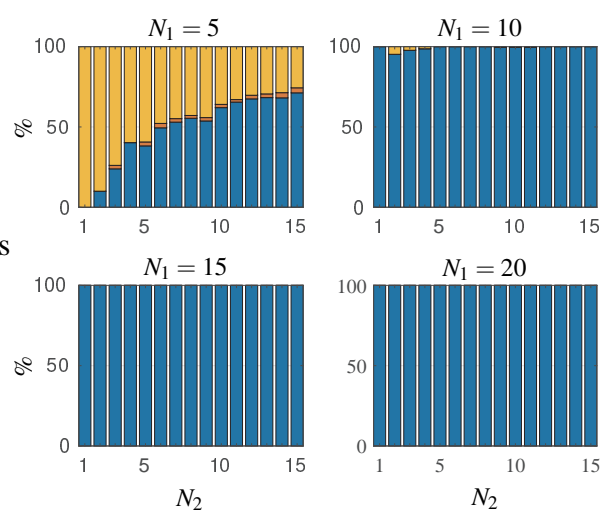


Figure 19. Model A, Experiment 4-1-3

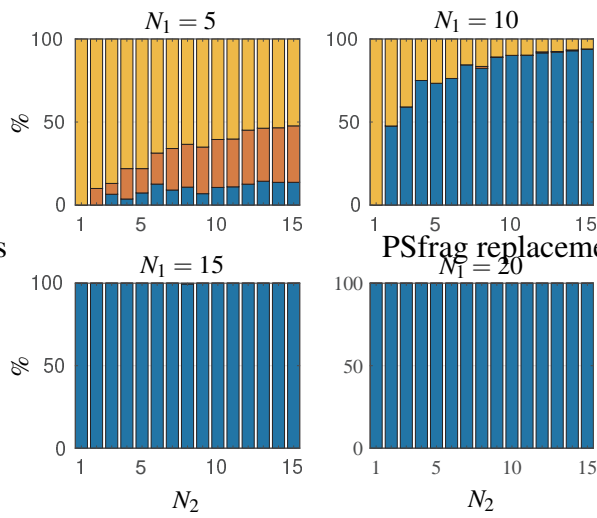


Figure 20. Model A, Experiment 4-1-5

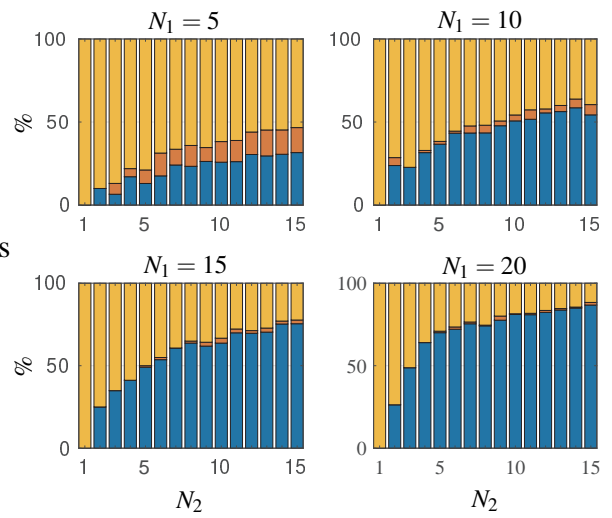


Figure 21. Model A, Experiment 4-2-1

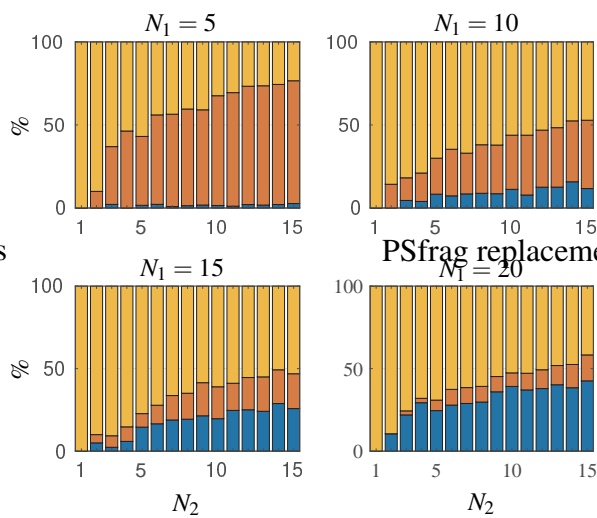


Figure 22. Model A, Experiment 4-2-3

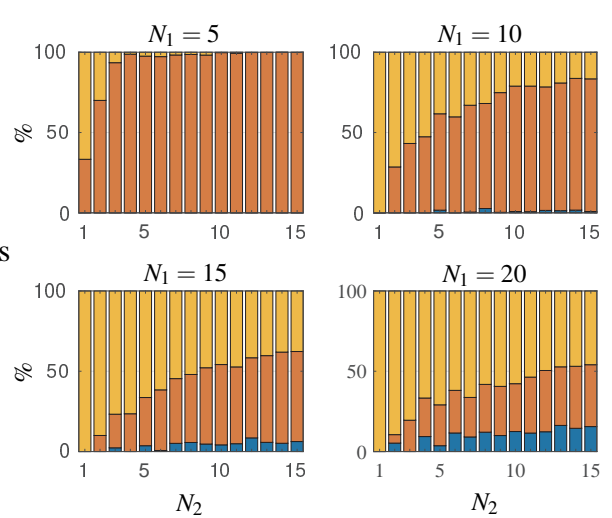


Figure 23. Model A, Experiment 4-2-5

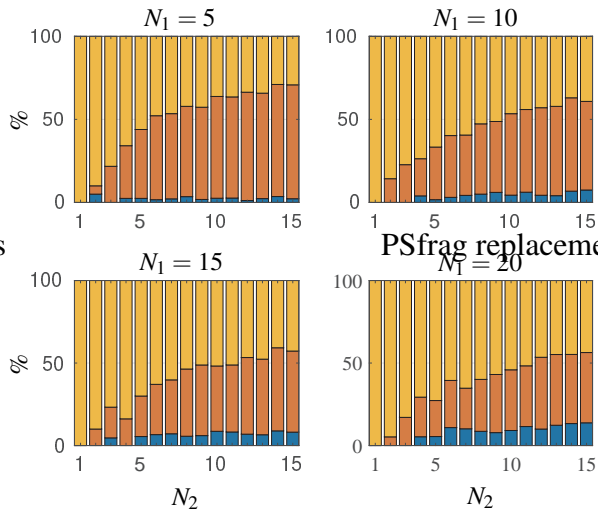


Figure 24. Model A, Experiment 4-3-1

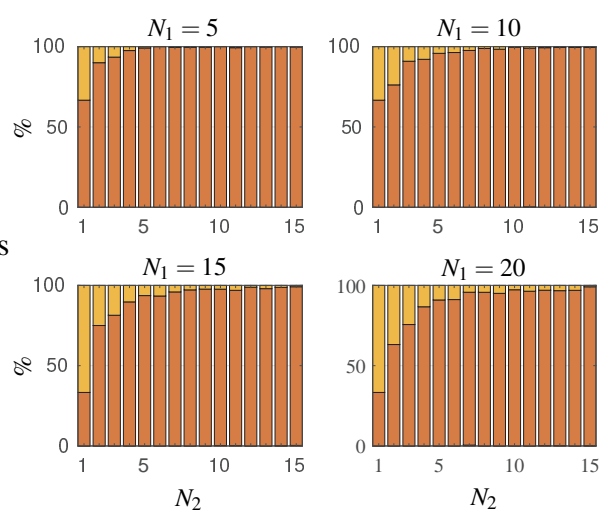


Figure 25. Model A, Experiment 4-3-3

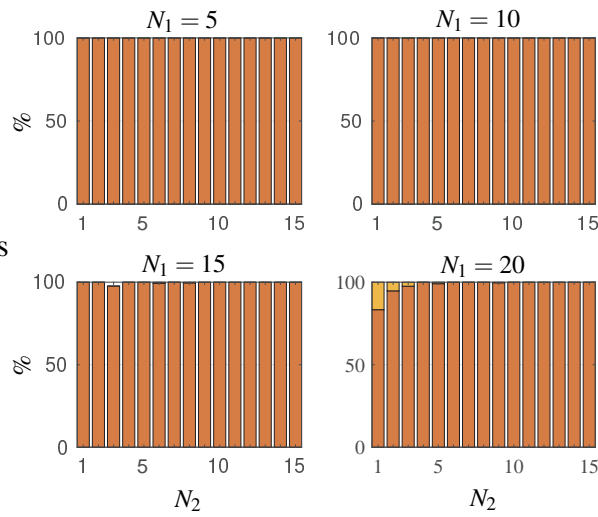


Figure 26. Model A, Experiment 4-3-5

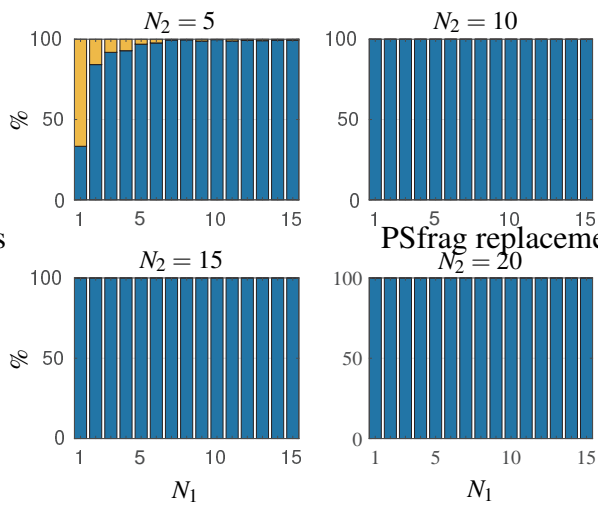


Figure 27. Model A, Experiment 5-1-1

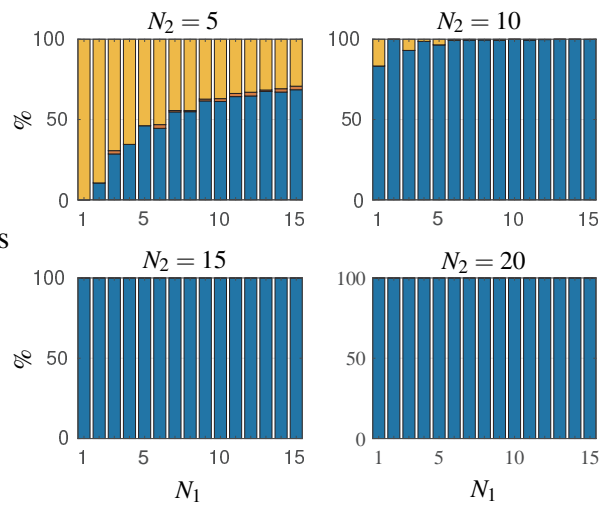


Figure 28. Model A, Experiment 5-1-3

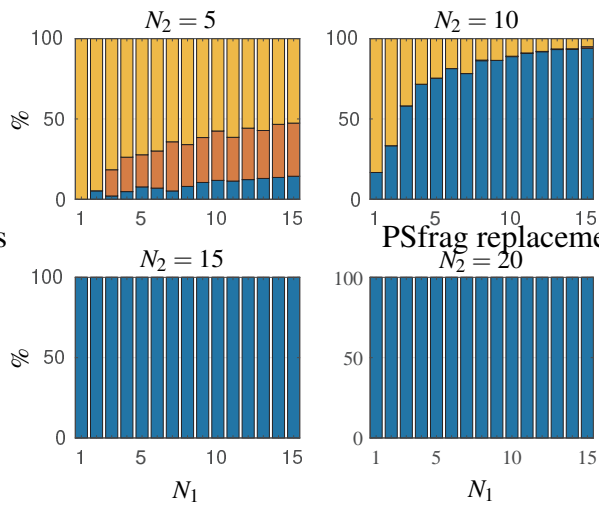


Figure 29. Model A, Experiment 5-1-5

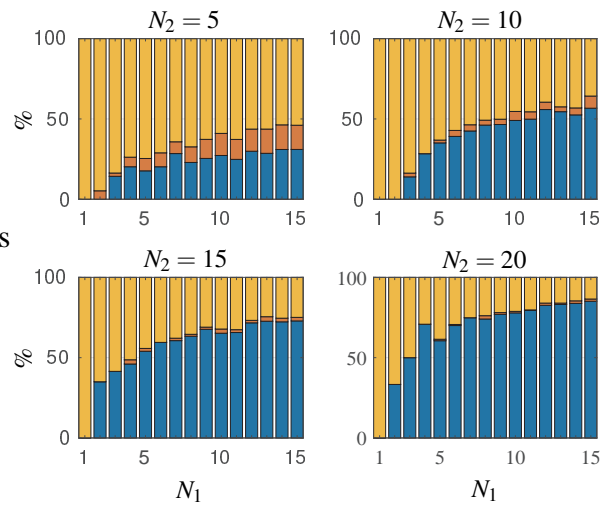


Figure 30. Model A, Experiment 5-2-1

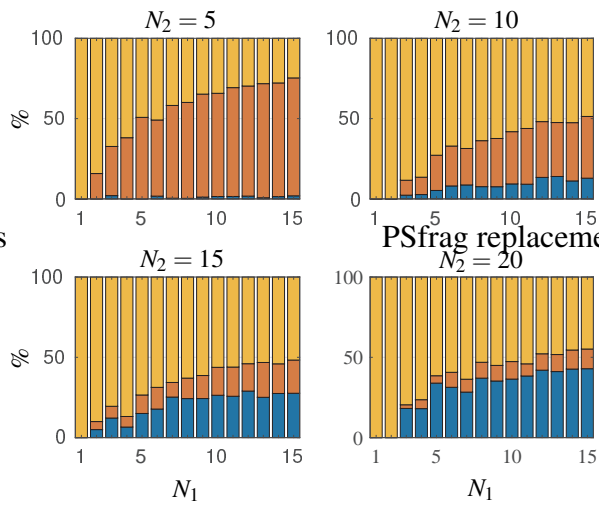


Figure 31. Model A, Experiment 5-2-3

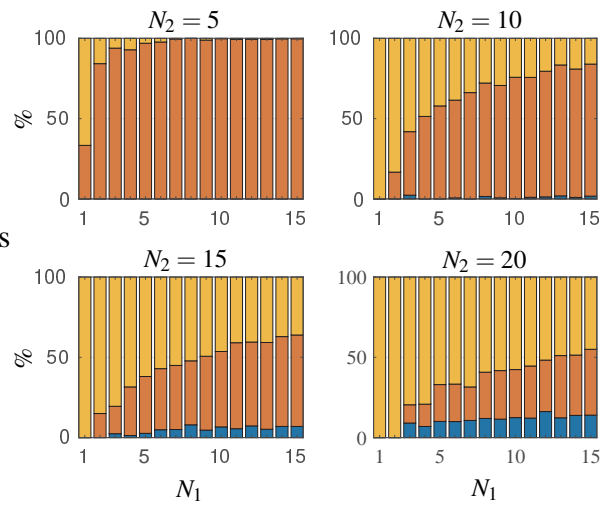


Figure 32. Model A, Experiment 5-2-5

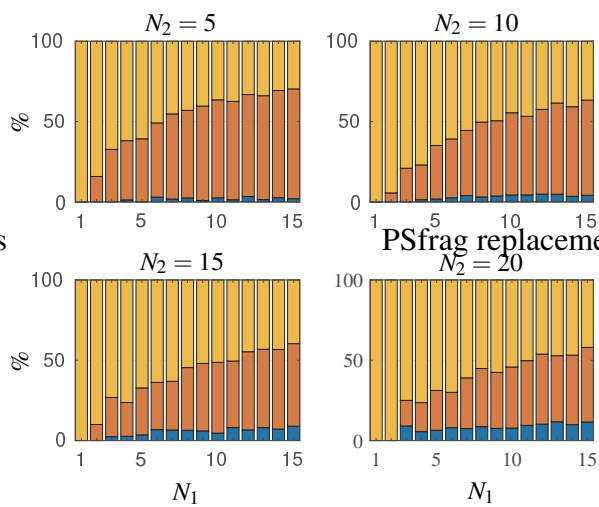


Figure 33. Model A, Experiment 5-3-1

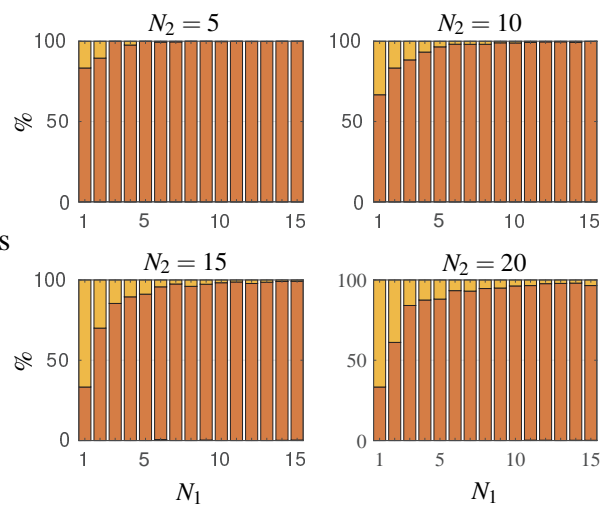


Figure 34. Model A, Experiment 5-3-3

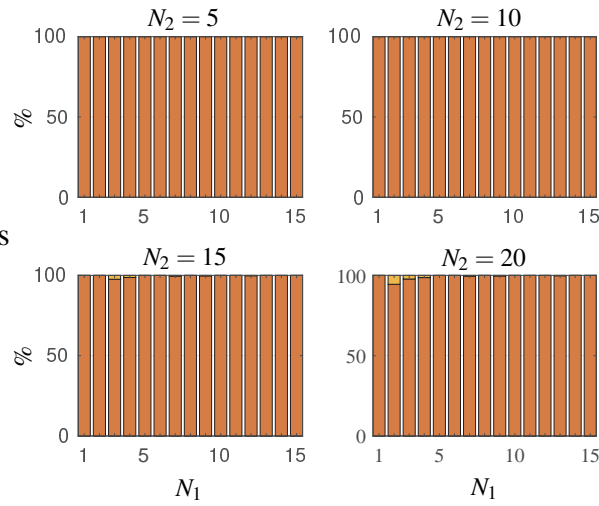


Figure 35. Model A, Experiment 5-3-5

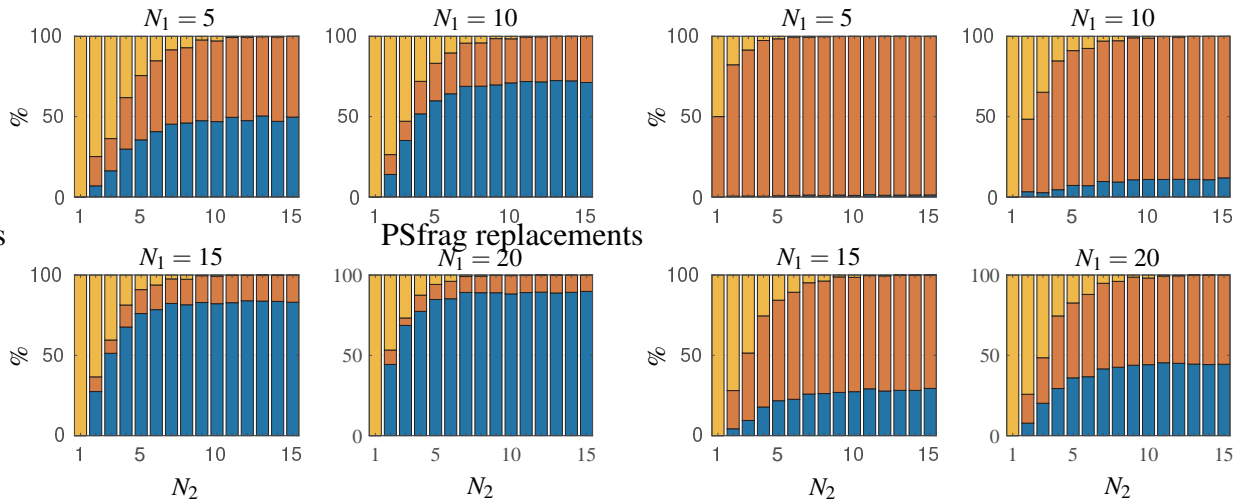


Figure 36. Model B, Experiment 4-1-1

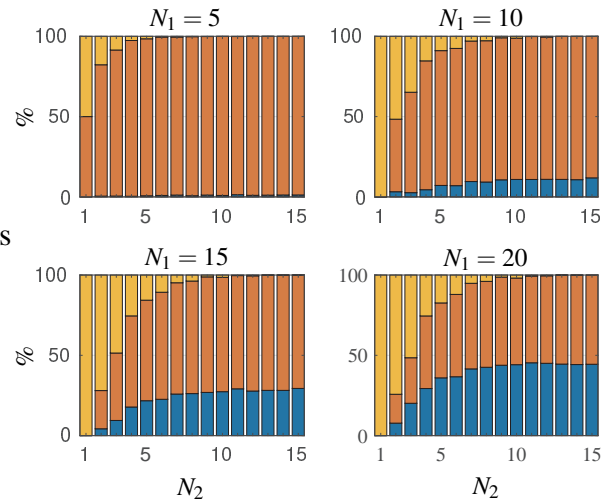


Figure 37. Model B, Experiment 4-1-3

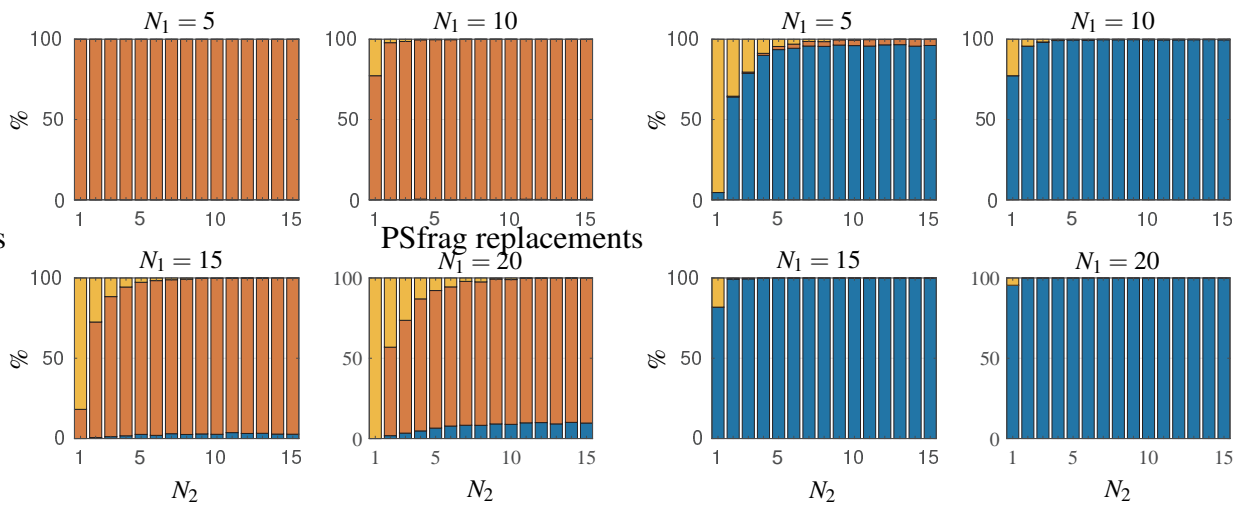


Figure 38. Model B, Experiment 4-1-5

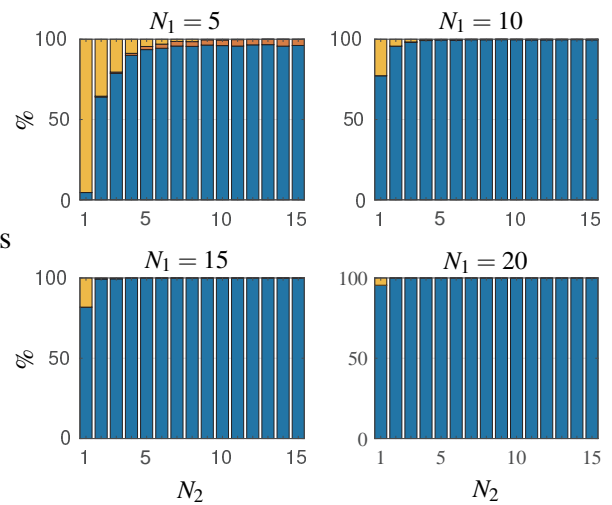


Figure 39. Model B, Experiment 4-2-1

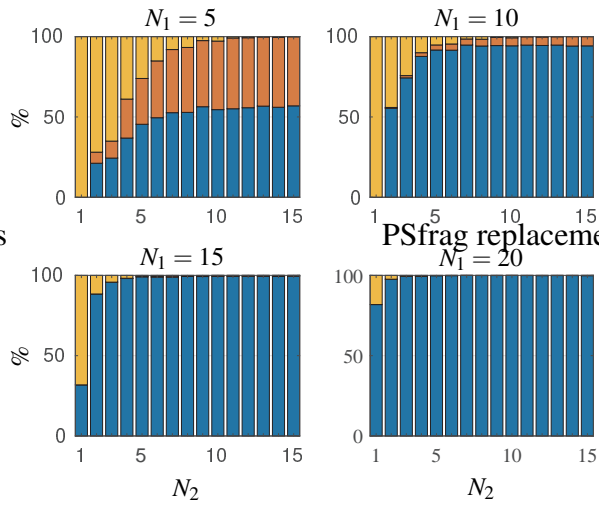


Figure 40. Model B, Experiment 4-2-3

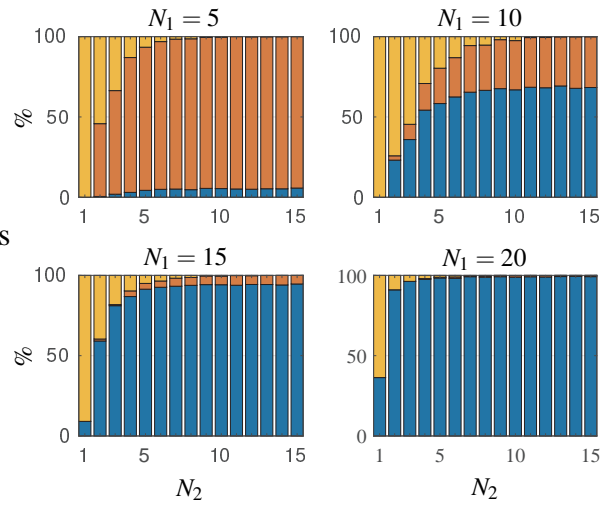


Figure 41. Model B, Experiment 4-2-5

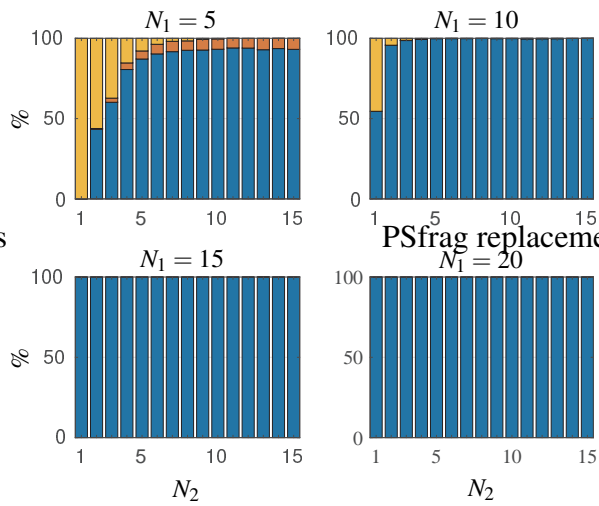


Figure 42. Model B, Experiment 4-3-1

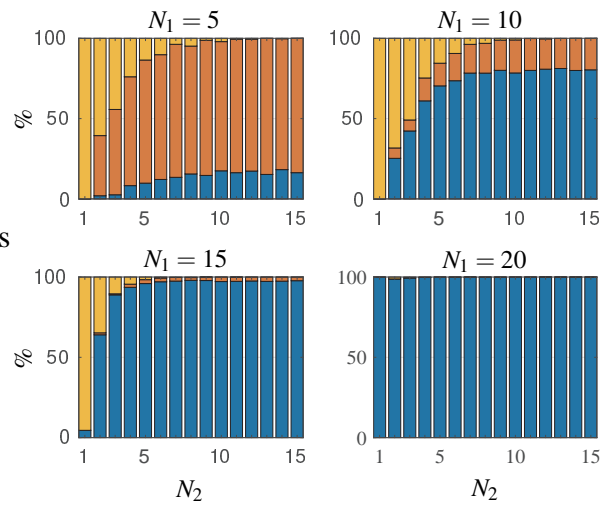


Figure 43. Model B, Experiment 4-3-3

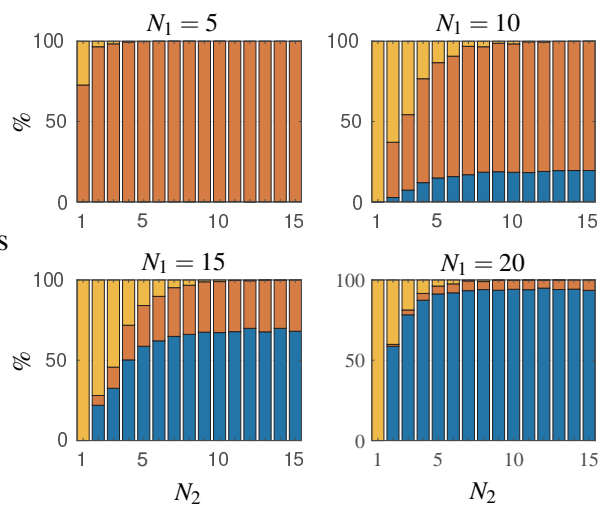


Figure 44. Model B, Experiment 4-3-5

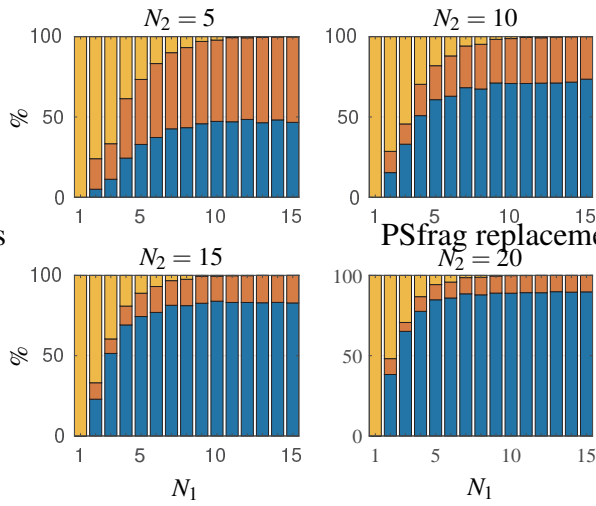


Figure 45. Model B, Experiment 5-1-1

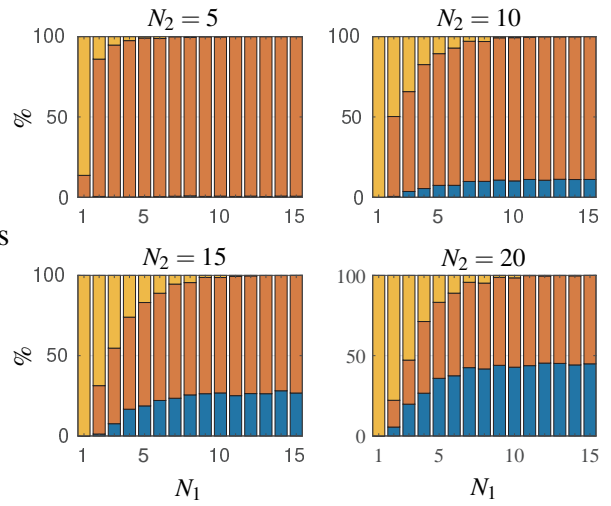


Figure 46. Model B, Experiment 5-1-3

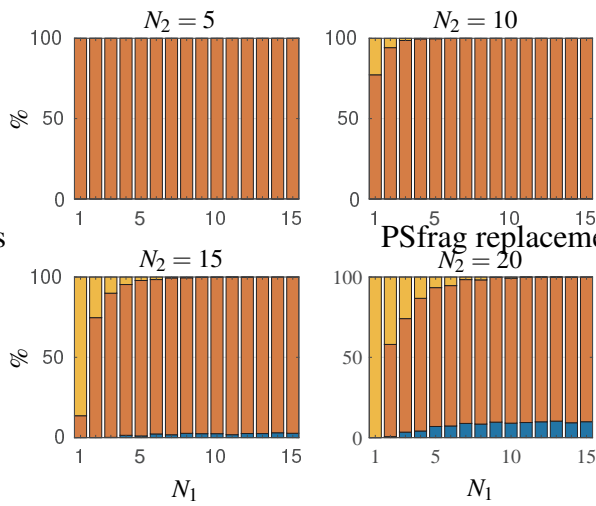


Figure 47. Model B, Experiment 5-1-5

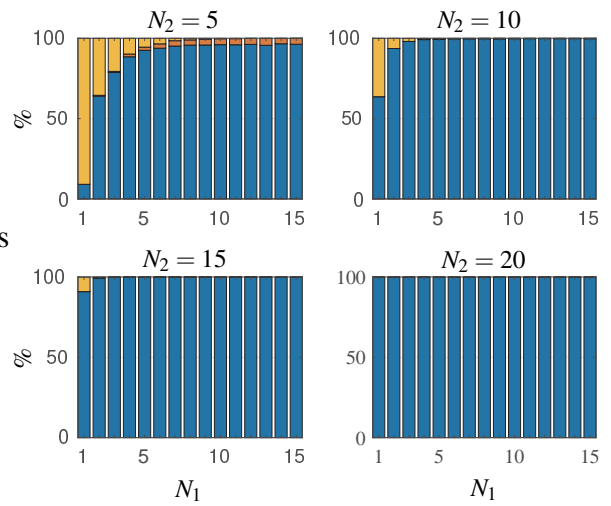


Figure 48. Model B, Experiment 5-2-1

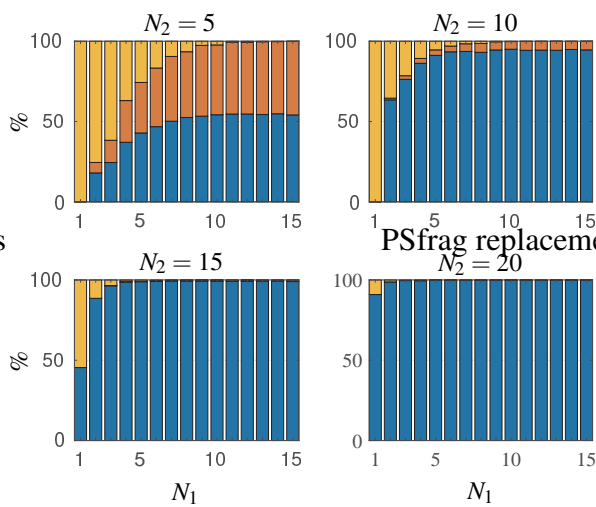


Figure 49. Model B, Experiment 5-2-3

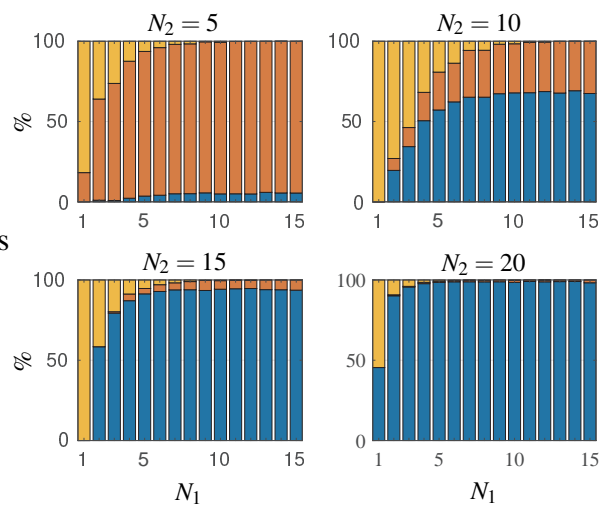


Figure 50. Model B, Experiment 5-2-5

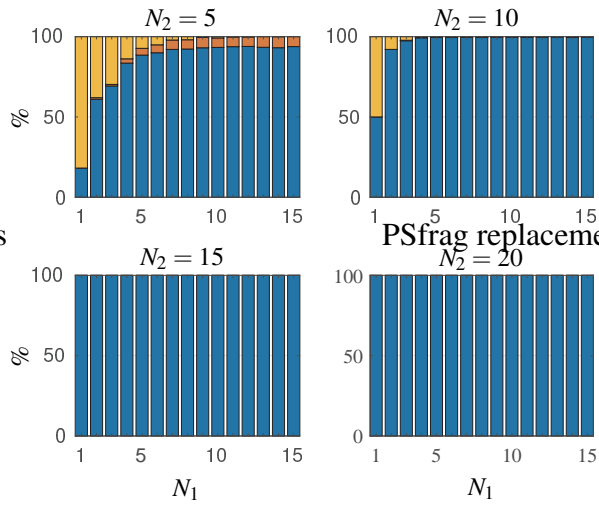


Figure 51. Model B, Experiment 5-3-1

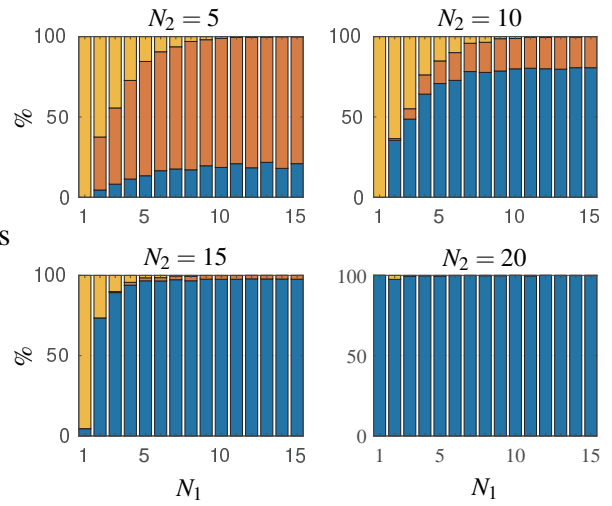


Figure 52. Model B, Experiment 5-3-3

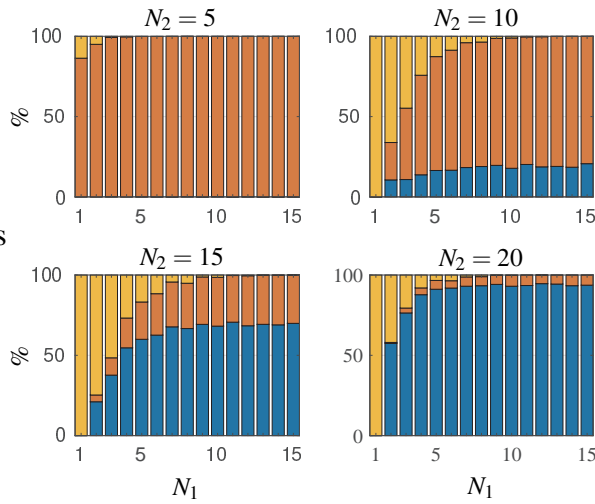


Figure 53. Model B, Experiment 5-3-5

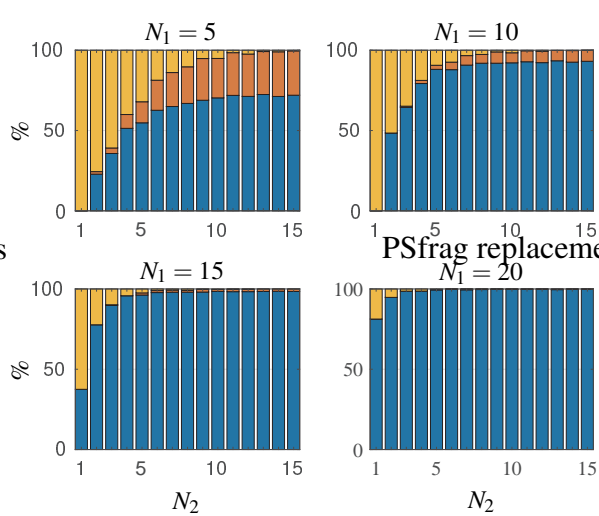


Figure 54. Model C, Experiment 4-1-1

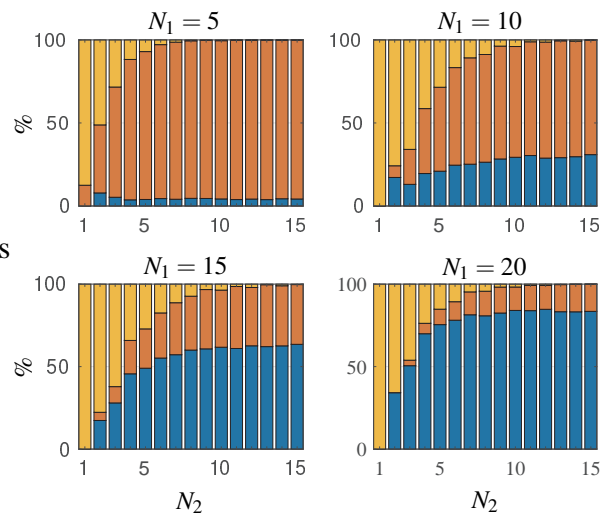


Figure 55. Model C, Experiment 4-1-3

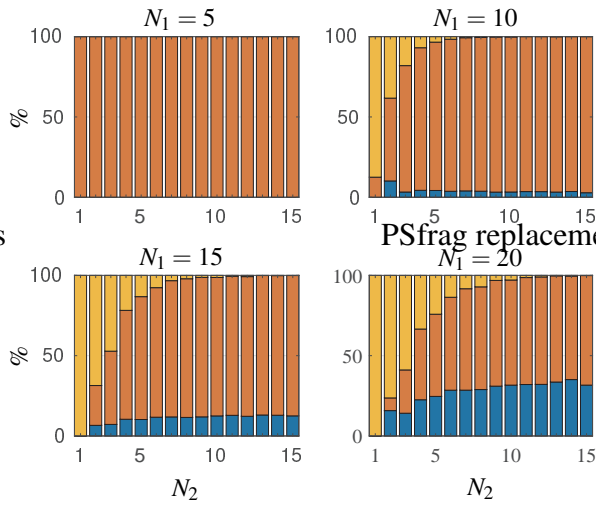


Figure 56. Model C, Experiment 4-1-5

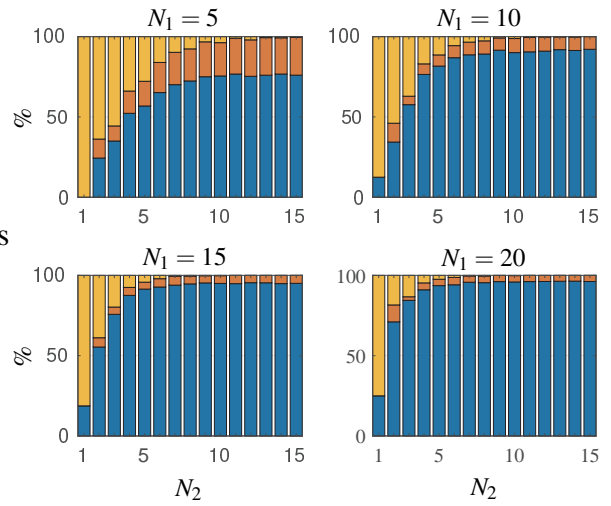


Figure 57. Model C, Experiment 4-2-1

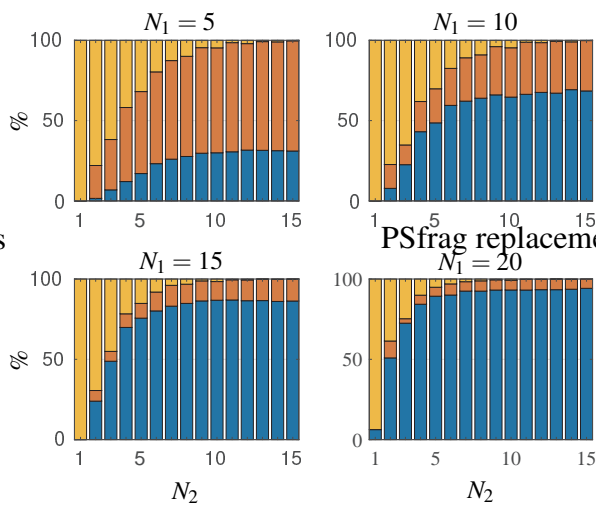


Figure 58. Model C, Experiment 4-2-3

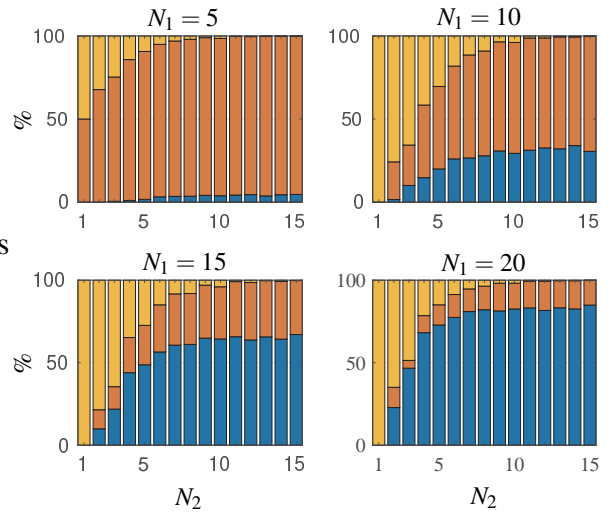


Figure 59. Model C, Experiment 4-2-5

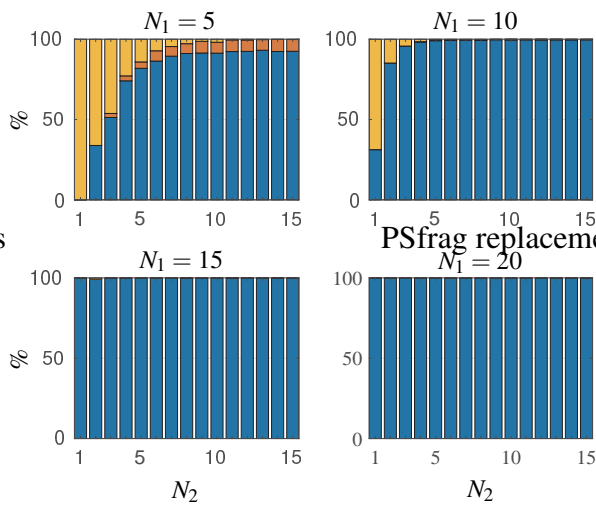


Figure 60. Model C, Experiment 4-3-1

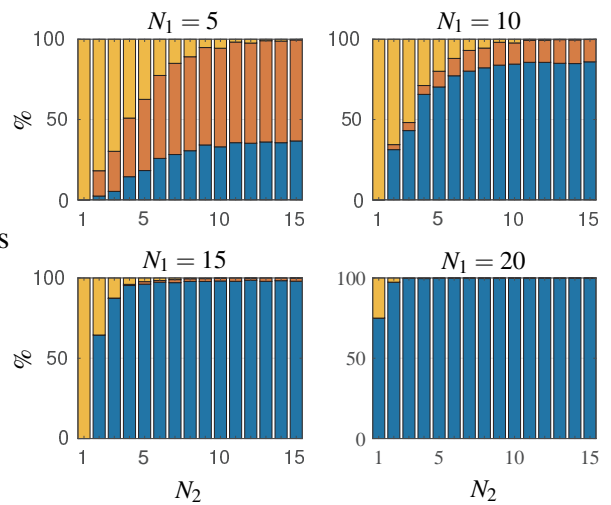


Figure 61. Model C, Experiment 4-3-3

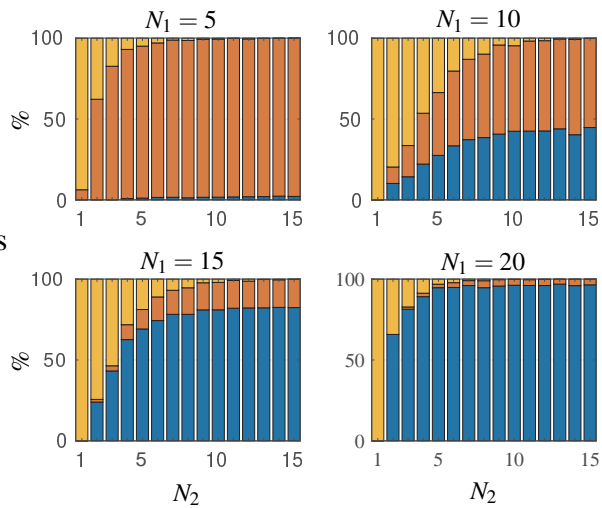


Figure 62. Model C, Experiment 4-3-5

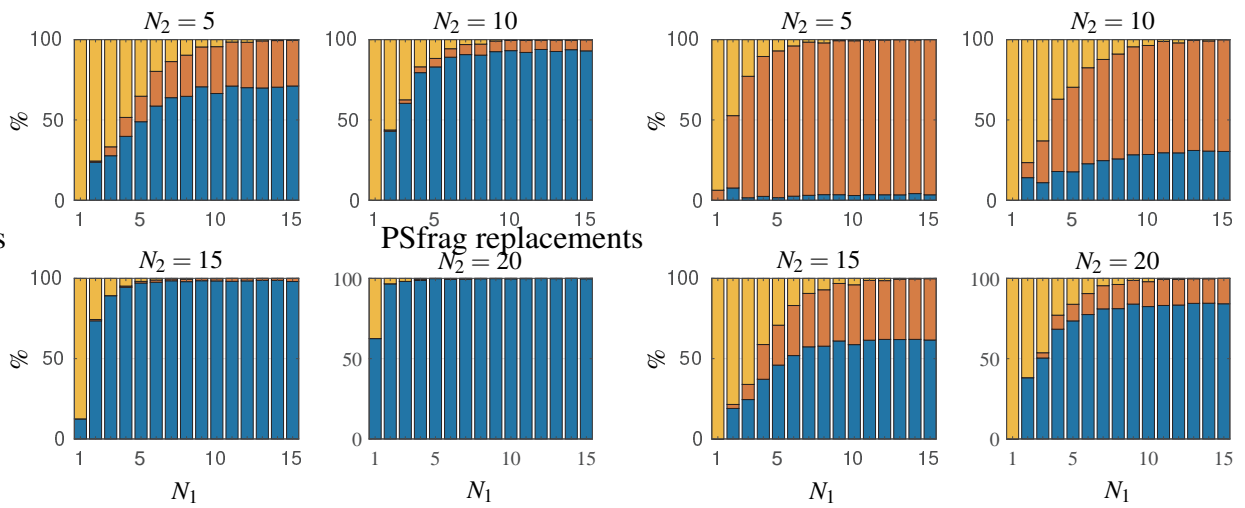


Figure 63. Model C, Experiment 5-1-1

Figure 64. Model C, Experiment 5-1-3

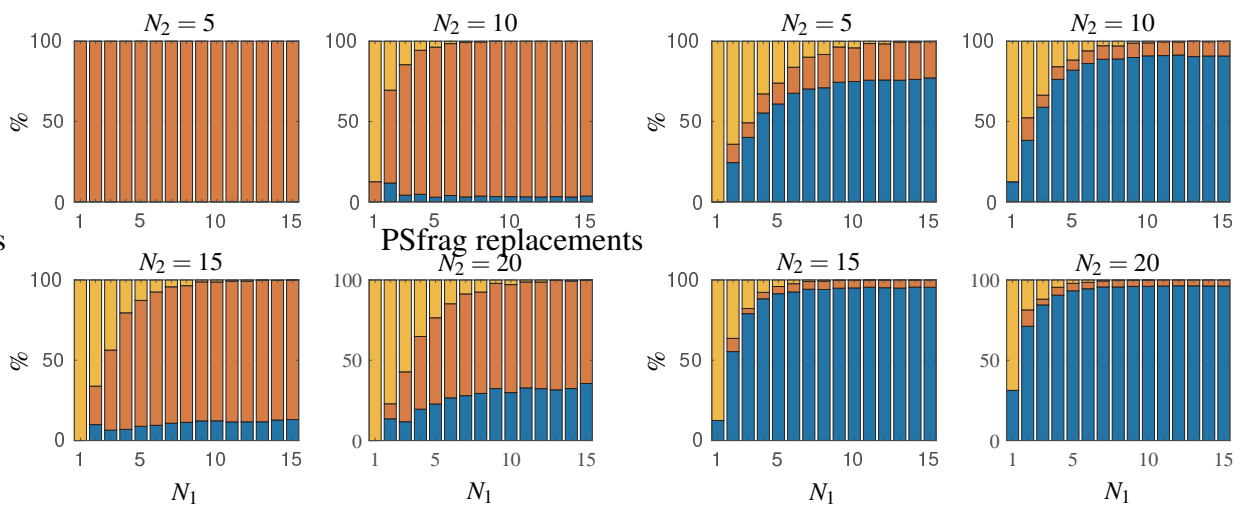


Figure 65. Model C, Experiment 5-1-5

Figure 66. Model C, Experiment 5-2-1

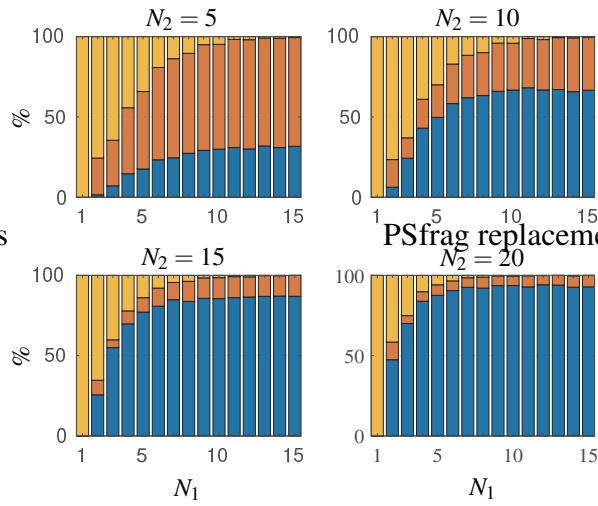


Figure 67. Model C, Experiment 5-2-3

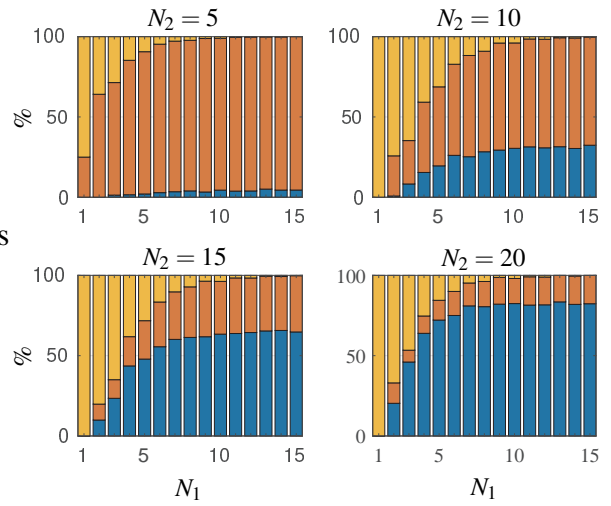


Figure 68. Model C, Experiment 5-2-5

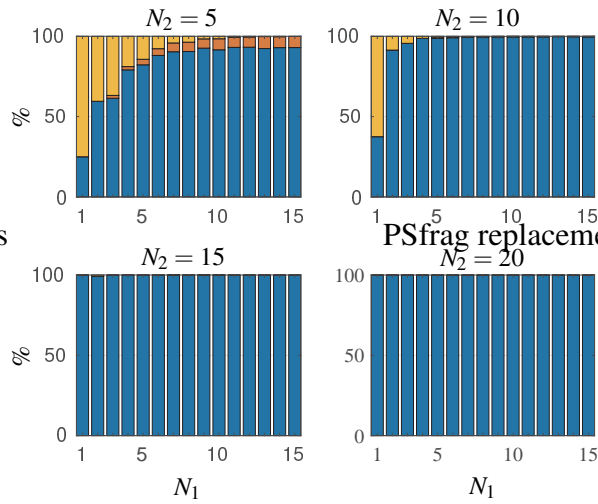


Figure 69. Model C, Experiment 5-3-1

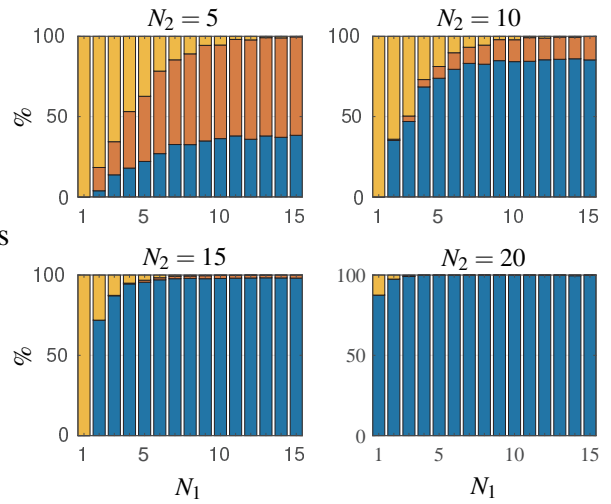


Figure 70. Model C, Experiment 5-3-3

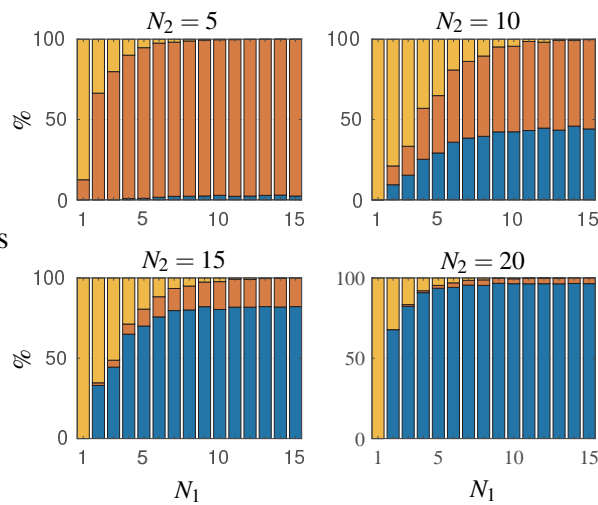


Figure 71. Model C, Experiment 5-3-5

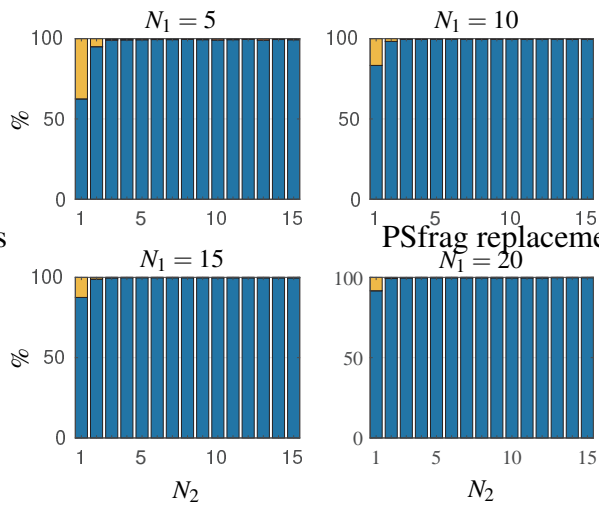


Figure 72. Model D, Experiment 4-1-1

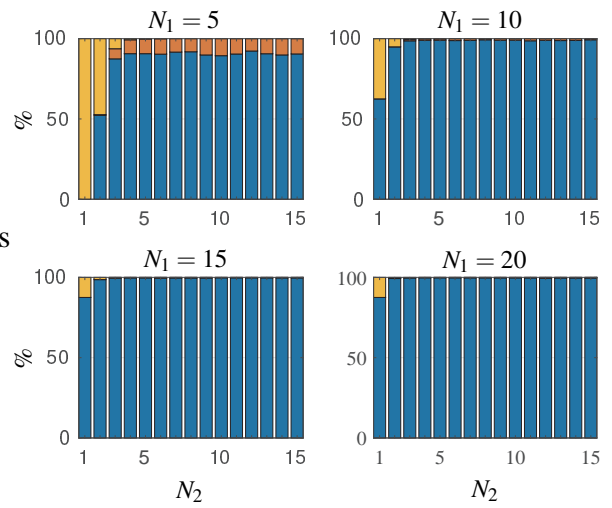


Figure 73. Model D, Experiment 4-1-3

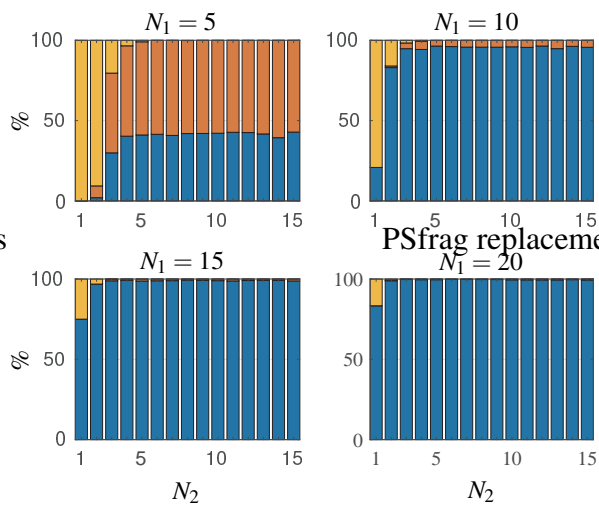


Figure 74. Model D, Experiment 4-1-5

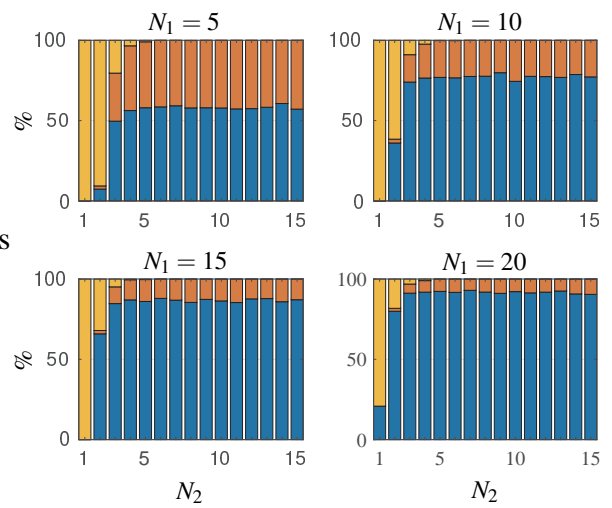


Figure 75. Model D, Experiment 4-2-1

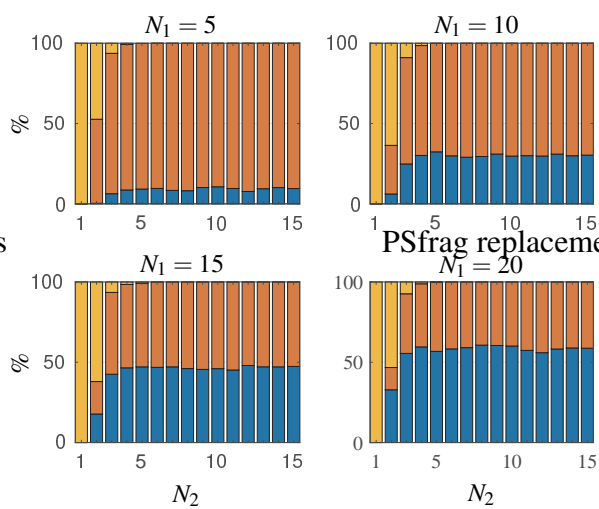


Figure 76. Model D, Experiment 4-2-3

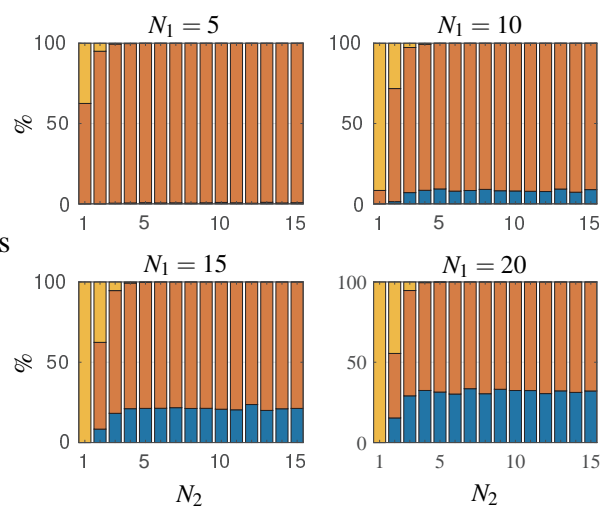


Figure 77. Model D, Experiment 4-2-5

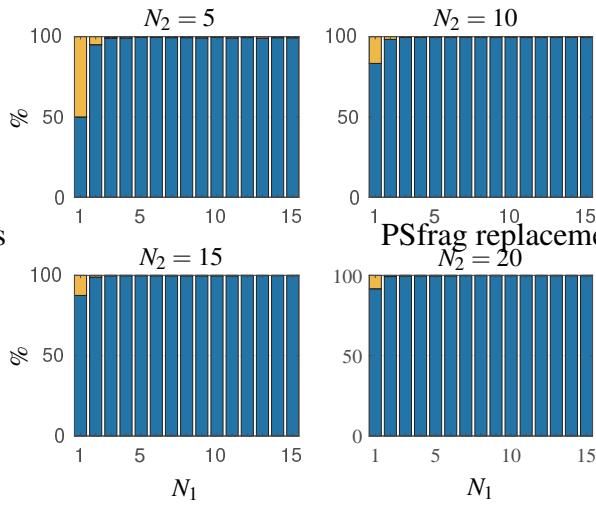


Figure 78. Model D, Experiment 5-1-1

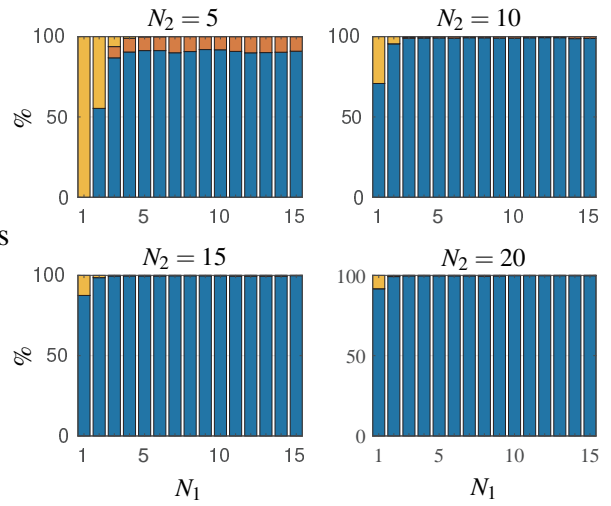


Figure 79. Model D, Experiment 5-1-3

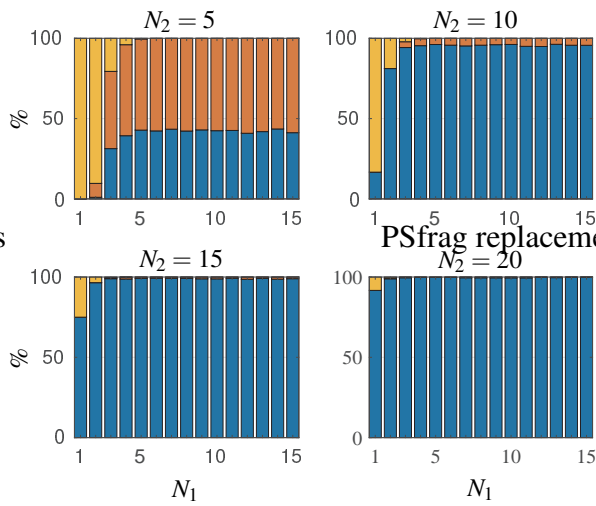


Figure 80. Model D, Experiment 5-1-5

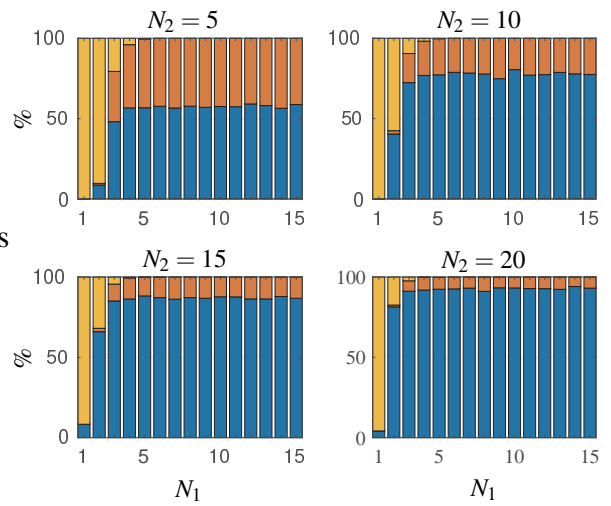


Figure 81. Model D, Experiment 5-2-1

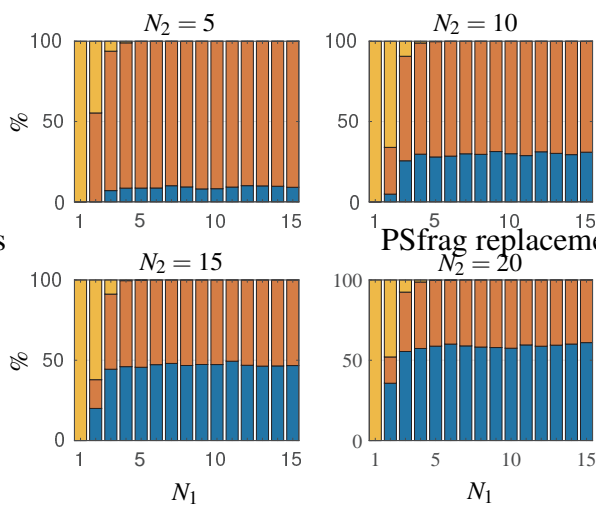


Figure 82. Model D, Experiment 5-2-3

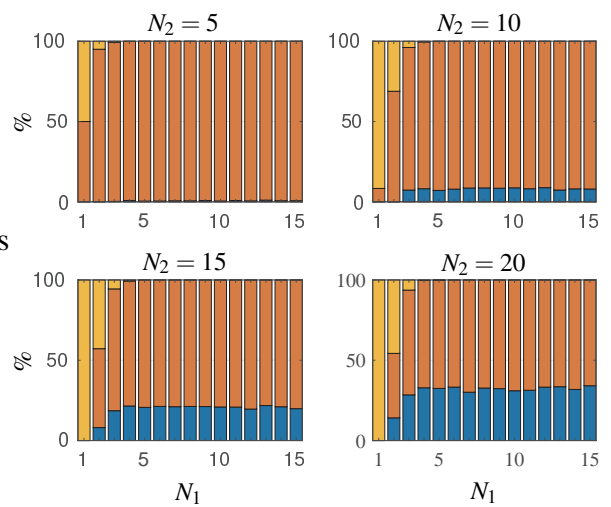


Figure 83. Model D, Experiment 5-2-5

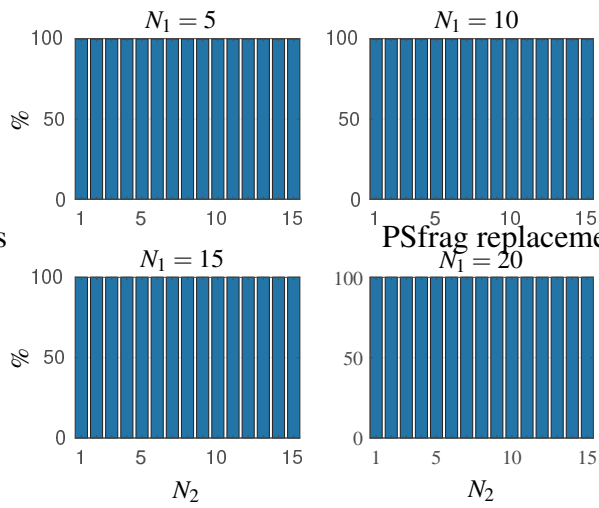


Figure 84. Model E, Experiment 4-1-1

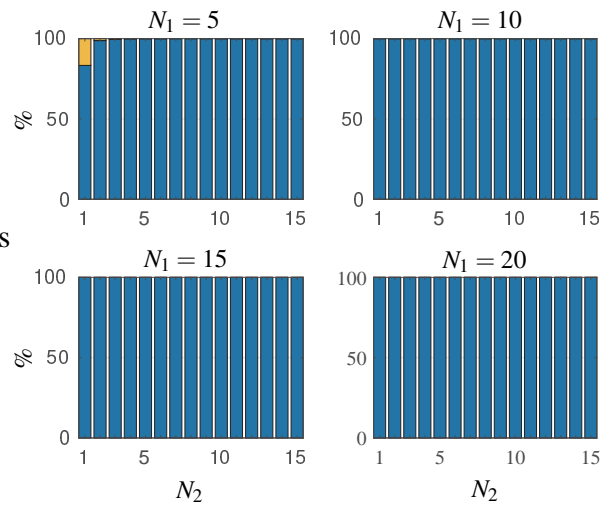


Figure 85. Model E, Experiment 4-1-3

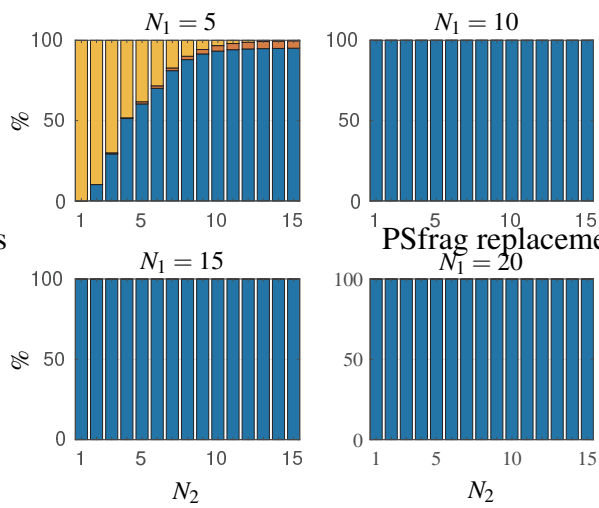


Figure 86. Model E, Experiment 4-1-5

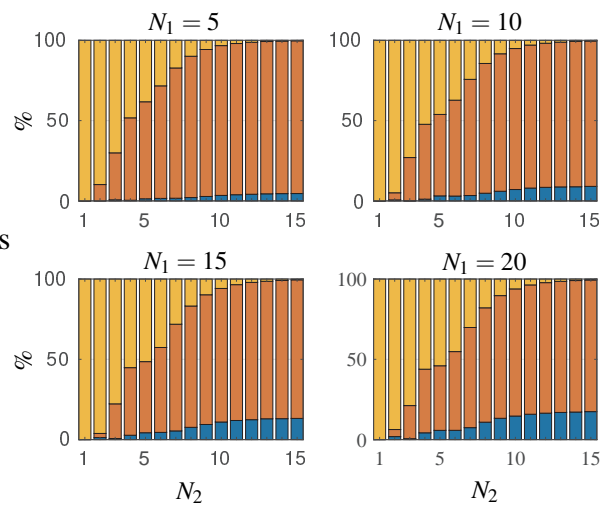


Figure 87. Model E, Experiment 4-2-1

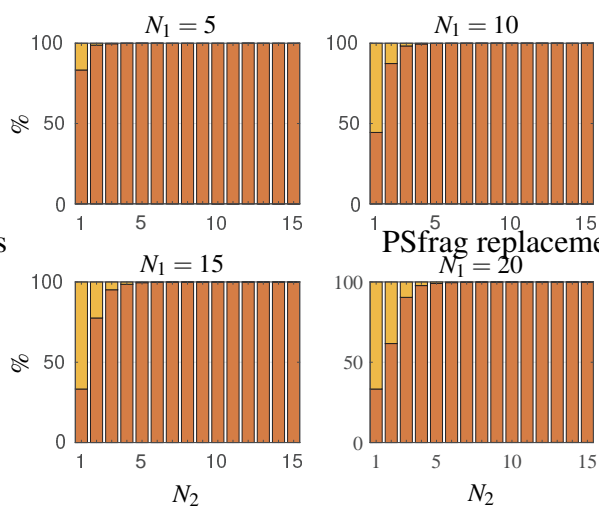


Figure 88. Model E, Experiment 4-2-3

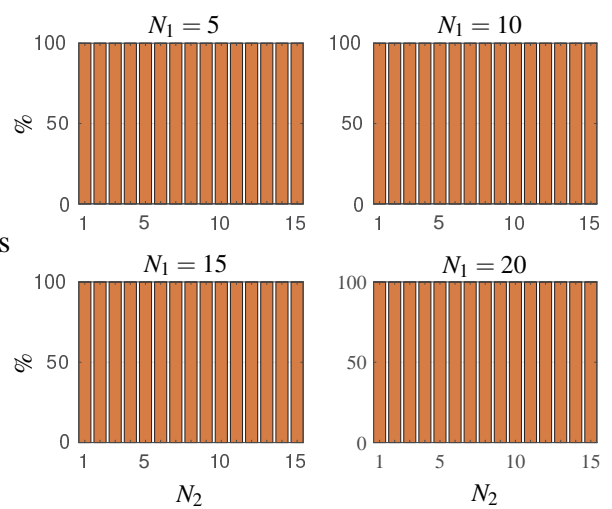


Figure 89. Model E, Experiment 4-2-5

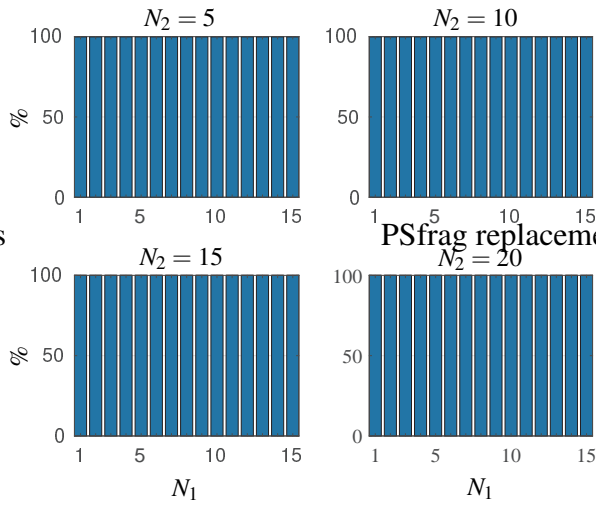


Figure 90. Model E, Experiment 5-1-1

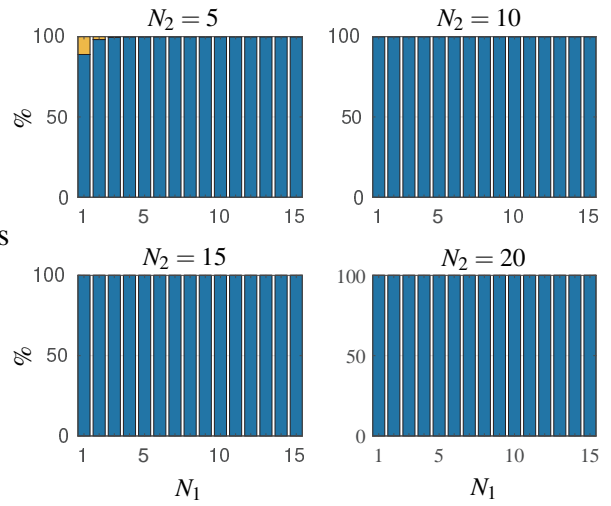


Figure 91. Model E, Experiment 5-1-3

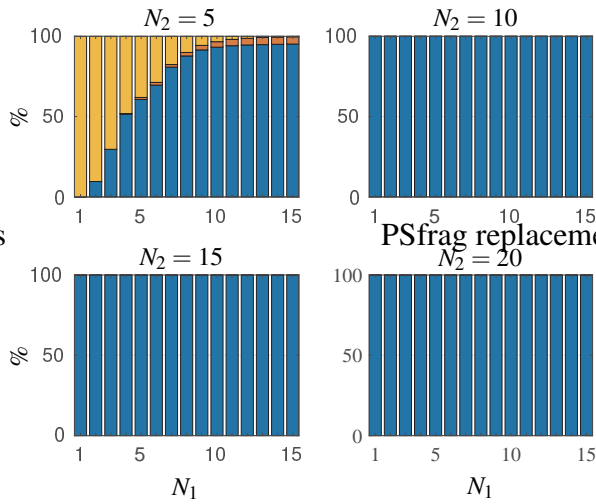


Figure 92. Model E, Experiment 5-1-5

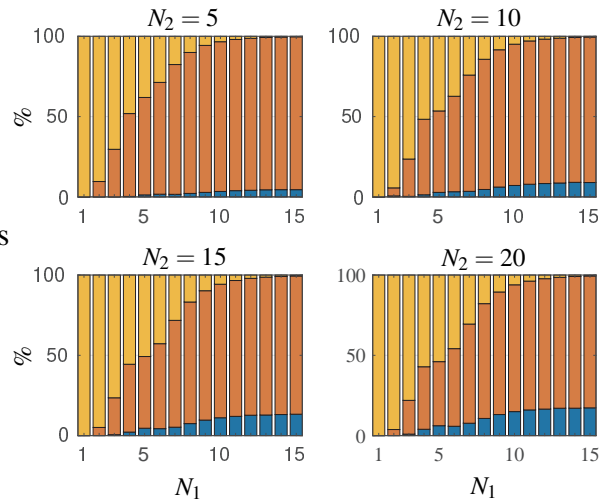


Figure 93. Model E, Experiment 5-2-1

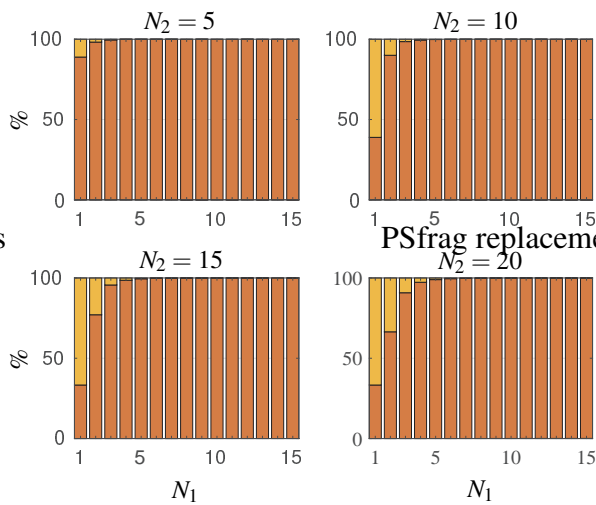


Figure 94. Model E, Experiment 5-2-3

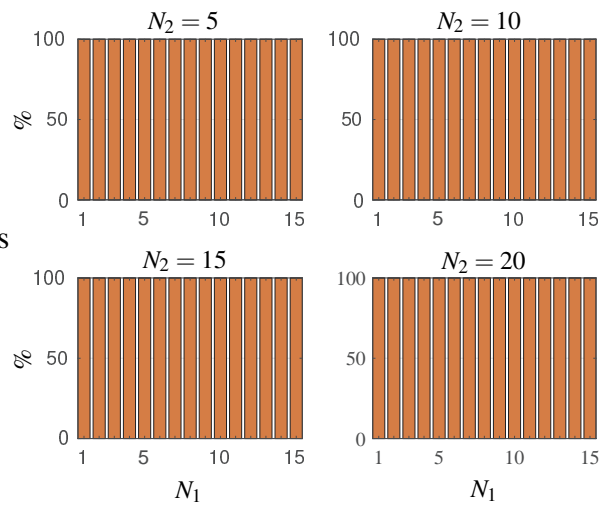


Figure 95. Model E, Experiment 5-2-5